Effects of prenylation inhibition on KRAS mutant tumors

PhD thesis

-CONFIDENTIAL-

Marcell Baranyi

Pathological Sciences Doctoral School

Semmelweis University

Supervisor: József Tímár, MD, DSc

Official reviewers: László Kőhidai, MD, CSc

István Szász, PhD

Head of the Complex Examination Committee:

Sarolta Kárpáti, MD, DSc

Members of the Complex Examination Committee:

Hajnalka Rajnai, MD, PhD

József Lövey, MD, PhD

Budapest

2022

Table of Contents

List of Abbreviations

4E-BP1	Eukaryotic translation initiation factor 4E-binding protein 1
70S6K	Ribosomal protein S6 kinase beta-1
A/B/CRAF	Rapidly accelerated fibrosarcoma (A/B/C)
AKT	Protein kinase B
AMP	Adenosine-monophosphate
ANOVA	Analysis of variance
ATCC	American Type Culture Collection
ATP	Adenosine-triphosphate
BAD	BCL2 associated agonist of cell death
BAX	Bcl-2-associated X protein
BCL-XL	B-cell lymphoma-extra large
BSA	Bovine serum albumin
CDC42	Cell Division Cycle 42
CI	Combination Index
CREB	cAMP Response Element-Binding Protein
DAPI	4',6-Diamidino-2-Phenylindole
DMEM	Dulbecco's modified Eagle's medium
DMSO	Dimethylsulfoxide
DNA	Deoxyribonucleic Acid
DTT	Dithiothreitol
EDTA	Ethylenediaminetetraacetic acid
EGF/EGFR	Epidermal growth factor / receptor
ELF4	74 Like ETS Transcription Factor 4
ERK	Extracellular signal pathway regulated kinase
FBS	Foetal bovine serum
FDA	Food and Drug Administration
FKB derived DD	Dimerization domain of FK506 binding protein
FTi	Farnesyl-transferase inhibitor
GAP	GTPase activating protein
GDP	Guanosine 5'-Diphosphate
GEF	Guanine nucleotide exchange factor

GFR	Glomerulus filtration rate
GGTi	Geranylgeranyl-transferase inhibitor
GPCR	G-protein-coupled receptor
GTP	Guanosine 5'-Triphosphate
HER1/2	Human epidermal growth factor receptor 1/2
HMG-CoA	3-hydroxy-3-metilglutaryl coenzyme A
HRAS	Harvey rat sarcoma viral oncogene homolog
HSP	Horseradish peroxidase
HVR	Hypervariable region (of Ras proteins)
ICMT	Isoprenylcysteine carboxy methyltransferase
IPP	Isopentenyl pyrophosphate
KRAS	Kirsten rat sarcoma oncogene homolog
LUAD	Lung adenocarcinoma
LZTR1	Leucine zipper-like transcriptional regulator 1
MAPK	Mitogen-activated protein kinase
MEK	Mitogen-activated protein kinase kinase
mRNA	Messenger ribonucleic acid
MTOR	Mammalian target of rapamycin
MYC	MYC Proto-Oncogene, BHLH Transcription Factor
NEDD41	Neural precursor cell expressed developmentally down-regulated protein 4
NRAS	Neuroblastoma v-ras (viral rat sarcoma) oncogene homolog
P53	Tumor protein p53
PAGE	Polyacrylamide gelelectrophoresis
PARP	Poly (ADP-ribose) polymerase
PBS	Phosphate-buffered saline
PCNA	Proliferating cell nuclear antigen
PDK1	3-phosphoinositide-dependent protein kinase 1
PDL1	Programmed death-ligand 1
PH	Pleckstrin homology (domain)
PI3K	Phosphatidylinositol-3-kinase
PIP2	Phosphatidylinositol 4,5-bisphosphate

PIP3	Phosphatidylinositol 3,4,5-trisphosphate
PKC	Protein kinase C
PLC	Phospholipase C
PM	Plasmamembrane
polyHEMA	Polyhydroxyethylmethacrylate
PTEN	Phosphatase and tensin homolog
PTM	Posttranslational modification
PVDF	Polyvinylidene fluoride
RAC1	Rac Family Small GTPase 1
RALA/B	Ras-related protein A/B
RALGDS	Ral Guanine Nucleotide Dissociation Stimulator
RGL1/2/3	Ral Guanine Nucleotide Dissociation Stimulator Like 1/2/3
RAS	Rat sarcoma, oncogene
RBD	Ras binding domain
RCE1	Ras Converting CAAX Endopeptidase 1)
RHEB	Ras homolog enriched in brain
RHO A/B	Ras Homolog Family Member A
RPM	Round per minute
RTK	Receptor tyrosine kinase
S6	Ribosomal protein S6
SCID	Severe Combined Immunodeficient (mice)
SD	Standard deviation
SDS	Sodiumdodecylsulfate
SEM	Standard error of mean
SHP2	Src homology region 2 domain-containing phosphatase-2
SRB	Sulforodhamine-B
TCA	Trichloroacetic acid
TSC1/2	Tuberous sclerosis complex 1/2
TTBS	Tris-buffered saline supplemented with 1% Tween80
TUNEL	Terminal deoxynucleotidyl transferase
WNT	Wingless-Type MMTV Integration Site Family
WT	Wild type

ZA	Zoledronic acid/Zoledronate
β-TRCP1	β-Transducin Repeat-containing Protein 1

1. Introduction

Mutations of RAS genes are present in around 19% of all malignancies and thus they are among the most frequently mutated oncogenes in human cancer. Besides, mutant *KRAS* is known as the most common driver oncogene in lung, colorectal and pancreatic adenocarcinomas [1-3]. The RAS protein family has three clinically highly relevant members, namely N, H, and KRAS. *KRAS* is transcribed in two isoforms, KRAS4A and KRAS4B that only differ in their hypervariable regions (HVR). *RAS* family members are all small GTP-ase proteins that physiologically cycle between inactive GDP-bound and active GTP-bound states, regulated specifically by their GAP (GTPase Activating Protein) and GEF (Guanin nucleotide Exchange Factor) proteins [4]. Oncogenic mutations occur mostly in three main hotspot sites including codons G12, G13 and Q61. These mutations result in impaired intrinsic GTPase activity and also prevent GAP regulator proteins in promoting hydrolyses of GTP to GDP. As a consequence, RAS proteins will be constitutively in active, GTP bound state [1]. Though sequences of the RAS proteins show high uniformity, differences can be found not only between sequences of the HVR (166-185 aa) but also in the catalytic domain. The catalytic domain consists of two lobe: lobe 1 shows 100% homology among all *RAS* genes (1-86 aa), while site specific amino-acid variations can be found in lobe 2 (87-171) that may influence intramolecular dynamics [5] and are also affected by rare mutations (e.g. codon 117 and 146) [6, 7].

1.1 Regulation of RAS activation

RAS proteins function as binary molecular switches based on their two major conformations: GTP-bound ON, and GDP-bound OFF states. As essential components of various important signaling pathways, their activation and inactivation is tightly regulated [8]. They possess similar affinity towards GTP and GDP, however, they have a slow off-rate for GDP. Thus, despite the much higher cellular concentration of GTP, they remain in GDP bound state until GEF proteins facilitate GDP/GTP exchange [8, 9]. Activation of RAS proteins by GEFs happens at the plasma membrane upon upstream stimuli, by RTK or GPCR signaling, among others [8]. Upstream receptors recruits adaptor proteins like GRB2 to the plasma membrane following activation, which pass on the signal

through binding RASGEF proteins. GEFs, like SOS1 facilitate dissociation of the nucleotide bound by RAS [4, 8]. Interestingly, GEFs do not favor GDP or GTP bound RAS and exchange of GDP to GTP is only the result of the 10 fold higher plasma concentration of the latter [4]. GDP-GTP exchange triggers conformational changes in RAS proteins, allowing RAS effectors to bind and be activated by RAS through their RBD domains.

Switching of RAS proteins to OFF state also require facilitation by regulatory proteins (GAPs), like NF1 [4, 8]. These are also huge, multidomain proteins that trigger hydrolysis of GTP to GDP upon binding to RAS proteins. Of note, RAS proteins possess intrinsic hydrolytic activity, though it is a very slow process ($k_{hydrolysis} = 68x10^{-5}\ s^{-1}$) [9]. Thus, switching OFF RAS signaling depends on the activity of GAP proteins. As a proof of principle, hotspot mutations affect primarily codons that are implicated in GAP binding (G12) and GTP hydrolysis (Q61) and renders these proteins insensitive to GAP mediated inactivation [1, 9]. Mutation at these sites also diminish drastically intrinsic GTPase activity of RAS proteins [9]. Interestingly, KRAS G12C mutation was found to be an exception, as this mutational variant retains ~75% of intrinsic GTPase activity of wild type proteins [9].

Besides regulation of activation status of RAS, modulation of plasma membrane localization is also a potential regulatory mechanism of RAS signaling. RAS plasma membrane (later also referred as PM) association can be modulated by a variety of mechanisms: palmytoilation-depalmitoylation cycle mediates disposition from the PM to the Golgi in case of HRAS, NRAS and KRAS4A [10], and KRAS4B PM association can be weakened by phosphorylation of S181 at the polybasic motif in its HVR [11]. Also, calmodulin can extract and sequester KRAS4B through its prenylated C terminal region [12]. Furthermore, membrane composition seems to be a modulatory factor as distinct RAS genes show differential distribution between cholesterol rich lipid rafts, membrane domains containing PIP2 or phosphatidic acid content [13, 14].

1.2 RAS signaling in cancer at a glance

RAS proteins act as a regulatory hub of numerous important signaling pathways that affect key processes fueling cancer progression. At least 20 different pathways can be

associated with regulatory activity of RAS, including RAF/MEK/ERK; PI3K/AKT/MTOR; PLC/PKC and RAL signaling pathway, among others [8, 15]. Of note, aberrant activation of RAS proteins alters signalization of downstream pathways that often contributes to developing malignant properties and hallmarks of cancer.

RAS/MEK/ERK signaling route is one of the most studied pathways directly regulated by RAS. Briefly, GTP-bound RAS proteins foster homo- or heterodimerization and phosphorylation of RAF proteins that in turn activate MEK1/2. Activated MEK1/2 confers signal to ERK1/2 proteins that enter the nucleus and phosphorylate numerous transcriptional factors associated with proliferation, growth and survival [16]. Admittedly, outcome of hyperactivated RAS/MEK/ERK signalization is highly context dependent and it is oversimplifying to connect it with only one specific hallmark of cancer [17], however, *aberrant proliferation* is generally observed as a consequence of mutations on this pathway.

Also, mutations of RAS proteins are known to confer resistance to apoptosis, fostering survival in unfavourable environment. Traditionally, activation of PI3K/AKT/MTOR cascade is linked with *growth* and *survival* and indeed, aberrant signalization of this pathway often fuels these processes during cancer progression [16]. Similarly to RAS/MEK/ERK pathway, effects of signaling through this pathway is context dependent and cross-talk with other pathways leads to various outcomes [18]. RAS proteins are also directly involved in regulation of this signaling cascade, through activation of PI3K along with a specific activated RTK. Activated PI3K converts PIP2 to PIP3 at the plasma membrane. PIP3 will be bound by effector proteins like AKT or PDK1, which will lead to activation and phosphorylation of AKT. AKT is known to negatively regulate several pro-apoptotic proteins like BAD, BCL-XL, BAX or induce transcription of anti-apoptotic factors through CREB [19]. Besides, activated AKT phosphorylates and inhibits TSC1/2. TSC1/2 is known to be a negative regulator of MTOR signaling through blockade of RHEB activity, which is a small G-protein. Inhibition of TSC1/2 reliefs its negative signal on RHEB that will in turn activate mTORC1 complex. mTORC1 activation leads to elevated biosynthesis of proteins, lipids or ribosomes as well as to increased autophagy and changed mitochondrial metabolism partly blockade 4E-BP1 protein (inhibitor of eLF4 transcription factor) and phosphorylation of p70S6K [20].

Besides regulating cellular energetics through mTORC1, mutant RAS, and especially mutant KRAS alters metabolism by a variety of mechanisms. Notably, *KRAS* mutant tumors display increased autophagy (as mentioned above) and macropinocytosis [21]. Autophagy (more specifically, macroautophagy) is a catabolic process through which a double membraned vesicle (called autophagosome) encompasses cell components that are to be degraded, for example damaged proteins or even organelles. This autophagosome later fuses with lysosome creating a new organelle called autolysosome which breaks down surrounded macromolecules into monomers. These monomers can be recycled during anabolic processes. Similarly, macropinocytosis in *KRAS* mutant cells also generates intermediates to fuel biosynthesis of macromolecules required for growth and proliferation of tumor cells. Briefly, macropinocytosis is an endocytotic process during which large portion of the extracellular space is internalized into large vesicles. These macropinosomes go through a series of maturation processes and finally fuse with lysosomes, resulting in the degradation of extracellular materials into monomeric intermediates [21].

Moreover, mutant KRAS increases glucose uptake as well as flux through a various of metabolic pathways like nonoxidative arm of the pentose phosphate pathway, glycolysis and hexosamine biosynthesis pathway through elevated MYC level [21]. Of note, increased *MYC* expression can be a result of the hyperactivated RAS/MEK/ERK expression [22]. In summary, mutations in *KRAS* result in various metabolic alterations that makes tumor cells more adaptable to challenges derived from growth requirement and biomass production that is essential for maintaining sustained proliferation.

RAS proteins can also directly regulate cytoskeletal dynamics, migration and motility. One important effector is the downstream RAS/RAL pathway [23]. Contribution of RALA, but more prominently of RALB to invasion and metastatic capacity of cancer cells is well established in several *in vitro* and *in vivo* studies [23-26]. RAL proteins, similarly to RAS, are small GTP-ases that require specific GEFs and GAPs for regulation of their activity. Some direct activator of RALA/B are effectors of RAS proteins, like RALGDS, RGL1, RGL2 or RGL3, thus mutant RAS proteins are able to induce increased invasive and metastatic behavior of cancer cells through this pathway [23].

Finally, modulation of the immune microenvironment and evasion from immune suppression is also a specific hallmark of malignant tumors. Mutant KRAS can induce

tumor promoting inflammation and also shape the immune microenvironment through production of various cytokines [27]. Furthermore, through stabilizing *PDL1* mRNA, mutant KRAS further modulates immune evasion which is a crucial process in maintaining tumor growth and survival in the hosts [28]. Indeed, combination of KRAS G12C inhibitors with immune checkpoint inhibitors has been proven to be a successful approach experimentally [29] and its clinical applicability is under investigation [30].
In summary, hyperactivated RAS contributes to malignant progression through a number of well-defined signaling cascades. Successful targeting of these key oncogenes are of major importance; however, unique properties of the individual RAS isoforms complicate the development of effective strategies.

1.3 Distinct features of the RAS proteins

Many studies discuss unique features of NRAS, HRAS, KRAS4A and KRAS4B. The incidence and organ specificity of the oncogenic mutations is obvious; mutation of *KRAS* is the most predominant followed by *NRAS* and then *HRAS*.

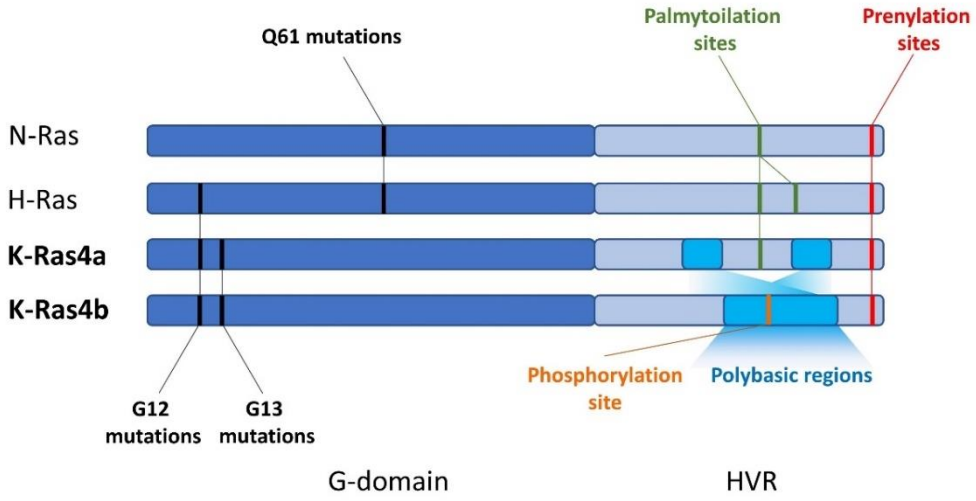

Figure 1 Most common oncogenic mutations and posttranslational modification sites of the HVR regions in the RAS proteins [31]

Interestingly, mutations in distinct *RAS* genes show tissue and codon specific patterns. For instance, *KRAS* is most frequently mutated in lung (~16%), colorectal (~30-34%) and pancreatic (~66%) adenocarcinomas. *HRAS* has the highest mutation rate in head and neck cancer and bladder cancer (5 and 7%, respectively) while *NRAS* mutations are

frequent in melanoma (~18%) [1, 2, 32]. *KRAS* mutations occur predominantly in codon G12 and G13 but *NRAS* is most commonly mutated in Q61. Interestingly, mutations of *HRAS* occur in codons G12 or Q61 at similar rates (**Figure 1)** [1].

Differential exposure to different carcinogens can be a possible explanation for distinct patterns of these mutations. For instance, G12C *KRAS* mutations in lung adenocarcinoma can be linked to smoking, while Q61 *NRAS* mutations in melanoma are associated with UV radiation. However, non-redundant functions of the distinct *RAS* family members may also be behind differences in mutational patterns [1].

Non-redundancy of *KRAS* was described in numerous studies. For example *HRAS* inserted to *KRAS* loci in mice can rescue lethal deficiencies in development, but ultimately give rise to cardiomyopathy, suggesting essential and distinct role for *KRAS* [33]. Furthermore, *NRAS* and *HRAS* were shown to be inessential for normal development as demonstrated by studies with knockout mice, while those with homozygous *KRAS* null mutation die between 12 and 14 days of gestation showing hematopoietic, neurological, liver and cardiac defects. Altogether, only *KRAS* seems to be indispensable for embryonic development [34-37]. Furthermore, HRAS was described to be a stronger activator of the PI3K pathway [38], while KRAS was shown to activate more dominantly the RAF/MEK/ERK pathway *in vitro* [39]. However, the fact that overexpression methods were used in these experiments should warn us to interpret these results with caution. More recently, using more precise genome editing strategies isogeneic cell lines were generated that carry mutations of distinct *RAS* genes expressed from their endogenous loci. These studies also establish differential signaling of the distinct RAS proteins, though these differences seem to be at a lower magnitude and depend more on the context than what was shown before [40].

Another study found that translation of KRAS was lower than of HRAS in human colorectal cancer cells, likely due to rare codon bias in *KRAS* sequence. Upon changing *KRAS* rare codons to common ones, *KRAS* expression increased. The authors hypothesize that the frequent *KRAS* mutations are due to the low KRAS expression, as higher levels may trigger oncogene induced senescence [41]. However, another study showed that expression of KRAS is higher than the other RAS proteins in all investigated tissue [42]. Besides, distinct features of the protein sequence of KRAS – that can be found mainly in the hypervariable region – are also expected to participate in its non-redundant roles.

1.4 Posttranslational modifications of RAS proteins

HVR region of RAS proteins is the most specific feature. A number of posttranslational modifications (PTM) affects this domain regulating RAS-membrane interactions. All RAS proteins have a CAAX motif at the C terminus which has a function in the regulation of prenylation. Prenylation is a PTM that consists of an irreversible attachment of a farnesyl (C15) or geranyl-geranyl (C20) lipid anchor to the 185 cystein (**Figure 1)**. Importantly, although they are preferably farnesylated, KRAS and NRAS (but not HRAS) protein can be subject alternatively to geranyl-geranylation (C20) when farnesylation is inhibited. [43]. Following attachment of the prenyl anchor, RCE1 enzyme cleaves the AAX motif. Ultimately, the C-terminus (C185) will be methylated by ICMT [44, 45].

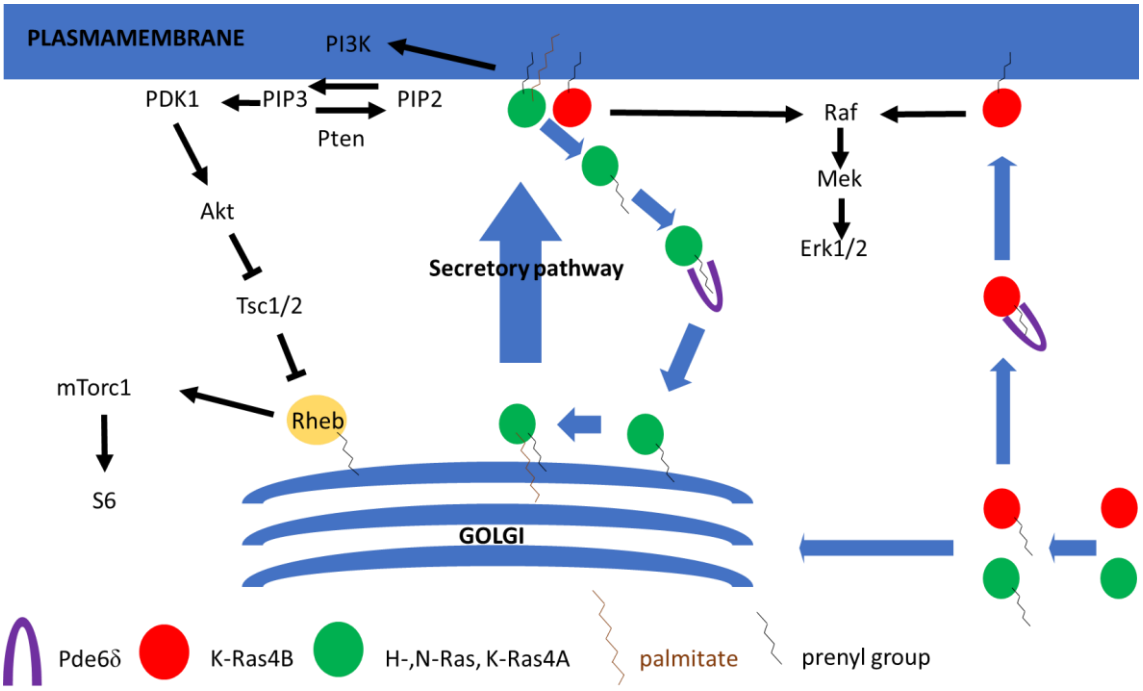

Figure 2 Schematic depiction of posttranslational modifications, traffic and localization of different RAS proteins. Modified after [46]

Specific features of HVR region of the KRAS isoforms (**Figure 1)** have distinct outcomes in membrane targeting (**Figure 2**). KRAS4A – as N and HRAS – can be subject to palmitoylation which is also a membrane-anchoring lipid modification, KRAS4B can only be prenylated [10]. In addition, KRAS4B also has a specific polybasic sequence in the HVR that facilitates protein-membrane interaction through the acidic regions of the

plasma membrane (PM) [47]. Phosphorylation of S181 that can be found within the polybasic sequence can further regulate association of KRAS4B with the PM [11].

Though KRAS4B is recognized as the major isoform, a recent study showed that KRAS4A is also commonly expressed and thus can also contribute to tumor progression. Interaction of KRAS4A with the PM – like N and HRAS – can also be regulated by palmitoylation [48]. Palmitoylation occurs in the in the Golgi apparatus and facilitates delivery of KRAS4A to the plasma membrane by vesicular transport. Of note, palmitoylation is a reversible modification, and indeed, depalmitoylation at the plasma membrane can transfer KRAS4A back to the Golgi (**Figure 2**).

Interestingly, KRAS4A contains also two clusters of basic residues at its HVR that are important – besides the above described palmitoylation-depalmitoylation cycle – for regulation of association with plasma membrane. Importantly, these clusters are not found in N and HRAS. Genetic modifications of either the palmitoylation site or the polybasic cluster results in the reduction of KRAS4A PM association. Introduction of the C186S mutation blocks prenylation, which in turn leads to dramatic inhibition of colony formation and reduction of ERK phosphorylation. This result suggests that prenylation is the most important PTM for KRAS4A protein to be fully functional [48].

1.5 KRAS targeting

As *KRAS* is one of the earliest oncogenes discovered, many attempts focused on blocking its oncogenic activity. Moreover, oncogenic mutations of *KRAS* are described as negative predictive factors for a number of targeted therapeutic approaches, e.g. to all anti-EGFR therapies or to bevacizumab, which is an anti-VEGF agent targeting angiogenesis [49-51]. However, it was soon declared "undruggable". In contrast to the successful targeting of ATP-binding sites of tyrosine-kinases, allosteric or competitive inhibition of KRAS is impeded by its compact nature, lack of targetable pockets and its picomolar affinity to GTP that is abundantly found in the cytoplasm [52]. One of the greatest steps were made recently by introducing KRAS G12C allele-specific inhibitors that broke the "undruggability" of RAS. These inhibitors specifically and covalently bind to the GDP-bound KRAS G12C protein and lock it at this inactive, "OFF" state. Sotorasib (AMG510), one of the most potent inhibitors has already been approved for treatment of lung adenocarcinoma carrying *KRAS* G12C mutation [53]. Nevertheless, resistance to

treatment with KRAS G12C inhibitors develops in the majority of patients [54]. Currently, various combinational approaches are tested in ongoing clinical trials that hopefully overcome this obstacle [54], however, new strategies are still urgently needed. Besides, other types of *KRAS* mutations (G12D, G12V, G13D or Q61) still lack targeted therapy, thus alternative approaches are under investigation for indirect inhibition. These attempts include targeting other proteins in RAS-controlled signaling pathways like MEK1/2 or PI3K; modulating regulatory proteins of RAS like SHP2 (of which exact biological function in this regard is yet to be established), blocking activity of SOS1, one of the most important GEFs of RAS proteins or targeting trafficking and localization of RAS [8, 52]. Interfering with trafficking of KRAS proteins can be achieved by targeting PDE6δ protein that is responsible for KRAS4B protein transport to the plasma membrane. Besides, PDE6δ is also function as a solubilizing agent of N/HRAS, promoting their localization to the endomembranes [8, 55]. However, blocking RAS PM localization is achieved primarily by blocking posttranslational modifications of the HVR region of RAS proteins [31].

1.6 KRAS localization in the regulation of signaling pathways

Though the process of posttranslational modification of KRAS had been well described it is still under debate whether its membrane anchorage is essential for functioning as a driver oncogene. This question is all the more compelling in light of numerous failures during the years in targeting KRAS prenylation.

First of all, it should be emphasized that a high complexity network, various important signaling cascades are regulated by KRAS proteins [15]. For the sake of perspicuity, we will further investigate the two most-studied signaling cascade that is under the regulation of RAS: the PI3K/AKT and RAF/MEK/ERK pathway.

In case of PI3K, association with the membrane is essential. Class IA PI3K consists of two subunits, the regulatory p85 and the catalytic subunit p110. PIP3 is created by PI3K upon phosphorylation of phosphoinositol molecules in the plasma membrane (PtdIns4P, PtdIns(4,5)P2). Effectors of PI3K (e.g. AKT, PDK1) upon binding to PIP3 through their pleckstrin homology (PH) domains, activate signaling cascades regulating numerous essential cellular activity like survival, motility, cell growth and proliferation [56]. Of importance, in order to reach full activation of PI3K, it was found to be vital to bind

concomitantly to autophosphorylated receptor tyrosine-kinases (RTKs) and to activated KRAS at the plasma membrane [57]. While it is evident that it is necessary for PI3K to be in association with the PM upon activation but - to our knowledge – no study investigated directly whether it is possible for PI3K to be activated by prenylation deficient KRAS (e.g C186S).

Regarding the RAF/MEK/ERK cascade, it is well established that dimerization of RAF is vital for its activation [58] and it was shown to happen at the plasma membrane [59]. Three homologous genes constitute the *RAF* family: *ARAF*, *BRAF* and *CRAF*. Following upstream activation, specific GEFs activate RAS by facilitating exchange of GDP to GTP. Activated, GTP-bound RAS recruits RAF via its RAS binding domain (RBD) and promotes their homo- or heterodimerization. BRAF/CRAF heterodimers are known as the most dominant formation for activation of downstream signaling. Dimerization fosters phosphorylation of RAF proteins, though it is still not known if it occurs by trans- or autophosphorylation. Phosphorylated RAF dimers pass on the signal to downstream effectors by phosphorylating MEK1/2. [60].

Interestingly, KRAS localization is not homogenous at the PM. Moreover, KRAS seems to signal through small clusters – nanoclusters - of RAS proteins at specific regions of the plasma membrane [13]. Recently, KRAS was found to be able to form homodimers [61]. As RAF activation occurs upon its homo- or heterodimerization and RAS-RAF interaction has a 1:1 stoichiometric ratio, it is possible that RAS dimerization precedes RAF activation physiologically. Indeed, efficacy of BRAF/CRAF heterodimerization and MAP kinase (MAPK) activation is diminished upon blocked KRAS dimerization or nanoclustering - either with specific antibodies or by genetic means [61, 62]. Of importance, another study has also proved that prenylation is essential for RAS dimerization dependent MAPK activation. They fused an FKB-derived dimerization domain (DD) to the N terminal of PamCherry1-KRas^{G12D}. Dimerization of these DDs can be induced with small molecule (that can link two DDs together). Addition of dimerizing agent resulted in KRAS dimerization and elevated MAPK activation. These effects could not be repeated using prenylation deficient C186S KRAS: addition of dimerization agent could induce neither KRAS dimerization nor activation of MAPK [63]. The KRAS dimerization interface is proposed to be between α-helix4 and α-helix5 of the opposite monomer. However, α-helix4 and α-helix5 interaction between two KRAS proteins are

relatively frail. Anchorage to the PM thus seems to be essential to foster higher local concentration of KRAS as well as their proper positioning so that dimerization can occur [61]. In addition, RAF membrane association has been shown to be facilitated by RAF cysteine-rich domains (CRD) that – along with RAS binding - maintain the signaling complex in association with the plasma membrane and - through reducing the RAS-RAF binding fluctuations – may enhance effective signaling [64].

1.7 Different classes of clinically applied prenylation inhibitors

Taken together, membrane anchorage of RAS – and so prenylation – seems to be essential for proper signal transduction based on available experimental data. For decades, KRAS was considered "undruggable" and thus its targeting was only feasible through blocking its membrane association. However, despite all promising preclinical data no clinical trial was proved to be successful.

In most of the cases, literature connects targeting prenylation of KRAS with the introduction and subsequent failure of farnesyl-transferase inhibitors (FTis). However, additional two types of clinically approved drugs should be mentioned in this regard as they also potently inhibit protein prenylation. These two drug classes are statins and nitrogen-containing bisphosphonates (N-bisphosphonates) [65]. Below, we will discuss briefly these three distinct classes of drugs concerning their mechanism and clinical applicability.

In contrast to statins and N-bisphosphonates, which are metabolic inhibitors, mechanism of action of FTis is fundamentally different. Through specifically inhibiting activity of the farnesyl transferase enzyme, FTis only block farnesylation resulting in narrower, less pleiotropic inhibitory effects than statins and bisphosphonates. Historically, farnesyltransferase inhibitors were predicted to block RAS activity, but clinical trials using FTis against *KRAS* mutant cancers turned out to be an often-cited failure. Subsequently, it was demonstrated that lack of efficacy on mutant KRAS can be explained by the fact that K and NRAS can be alternatively geranylgeranylated if farnesylation is blocked [65, 66]. However, FTis efficiently block prenylation of HRAS and other small G proteins that only capable of farnesylation [67]. Recently trials have been initiated investigating if tumors (head and neck and bladder cancer) carrying mutant HRAS – that can only be subject of farnesylation – can be targeted by FTis [31].

Statins block specifically the HMGCoA-reductase enzyme which function is to turn HMGCoA to mevalonate. Notably, this conversion is the rate-limiting move in the process of this metabolic pathway. Upon blocking synthesis of mevalonate, production of downstream derivatives is also inhibited. Indeed, depletion of mevalonate has been shown to be the primary mechanism of action, as demonstrated by rescue experiments where supplementation with exogenous mevalonate reverted inhibitory effects of statins [68]. Anti-cancer activity of statins has been demonstrated by many *in vitro* studies, which showed that statins exerted pro-apoptotic and anti-proliferative effects on various types of tumor cells.[69-72]. Underlying these activity, G1 and S-phase block was identified which is claimed to be mediated through blocking prenylation of cell cycle regulatory proteins [68]. Besides, RHO proteins are also commonly identified as primary target of statins [68].

Although statins are approved for treatment of hypercholesterolemia, there are some known difficulties that complicates their usability *in vivo.* First of all, dose-limiting toxicities may prevent achieving effective plasma concentration [68]. Second, it is well known that statins have a tendency for interacting with other drugs that can impede their usability in combination therapies due to toxic outcomes [73].

N-bisphosphonates – not like other bisphosphonates – have been demonstrated to block farnesyl-pyrophosphate synthase and – less effectively – geranylgeranyl-pyrophosphate synthase. Like in case of statins, this also leads to depletion of downstream metabolic derivatives. Supplementation with farnesyl-OH and geranylgeranyl-OH (pre-forms of farnesyl-PP and geranylgeranyl-PP, respectively) reverts the effects of N-bisphosphonates [74]. Of note, non-nitrogenous bisphosphonates have a markedly different mechanism of action, as their anti-tumor activity is carried out by accumulation of non-hydrolysable cytotoxic ATP analogues [75].

Nevertheless, anti-cancer effects of N-bisphosphonates that is mediated by prenylation inhibition are similar to those of statins. Pro-apoptotic, anti-proliferative effects of bisphosphonates have been demonstrated on cancers cells with different tissue of origin [76-83]. G1-S phase arrest could also be observed [84, 85]. Besides direct anti-cancer activity, bisphosphonates are considered as a potential modulator of tumor

microenvironment, for example through blocking osteoclast activity, potentiating gammadelta T cells or inhibiting angiogenesis [86, 87].

Importantly, due to their high affinity to mineral substance of the bones, applicability of bisphosphonates is limited for treatment of osteoporosis and bone metastases [88]. Additionally, bisphosphonates are considered to have favorable side-effect profiles, though high or frequent doses can result in the osteonecrosis of the jaw [89]. Besides, it should also to be noted that renal function with GFR>35ml/min is also required for administration of bisphosphonates [90]. Recently, lipophilic N-bisphosphonates have been successfully developed that show no affinity to bone material. These new drugs thus may be used for anti-cancer treatment in non-bone related conditions and may also not lead to osteonecrosis [91].

As statins and N-bisphosphonates both act as metabolic inhibitors of the mevalonate pathway, they are expected to have similar effects and outcomes, considering that intermediates between mevalonate and farnesyl-PP can be associated with no cellular processes. However, this seems not to be the case. For example, it was shown that N-bisphosphonates – through blocking transformation of IPP to farnesyl-PP – causes increase in the amount of IPP that in turn will be linked to AMP building up a cytotoxic ATP analogue ApppI [92]. Besides, interference with the mevalonate pathway on distinct levels may cause differential changes in the dynamics of synthesis of downstream substrates that could also affect outcomes. In addition, significant pharmacological differences also divide statins and N-bisphosphonates to two markedly different drug classes.

1.8 Consequences of prenylation inhibition

Approximately 2% of the proteome is subject to prenylation and many important regulatory proteins can be found among them that play essential roles in numerous cellular processes (**Figure 3**) [93]. These regulatory proteins involve many small GTPases, like CDC42 regulating cell cycle progression [94], RHEB taking part in the mTOR pathway that is associated with growth and metabolic regulation and RAC and RHO proteins modulating motility [95]. In this regard, our group has recently shown that the growth inhibitory effects of N-bisphosphonates can be associated with blocked RHEB prenylation [96]. Furthermore, several publication conclude that inhibitory potential of

statins or bisphosphonates are primarily based on blockade of RHOA/B prenylation [65, 68].

Besides, lamins, which are important components of the nuclear skeleton, are also prenylated proteins. Indeed, lonafarnib has been recently approved for clinical application treating progeria that is mainly associated with aberrant accumulation of prenylated pre-lamin proteins [97].

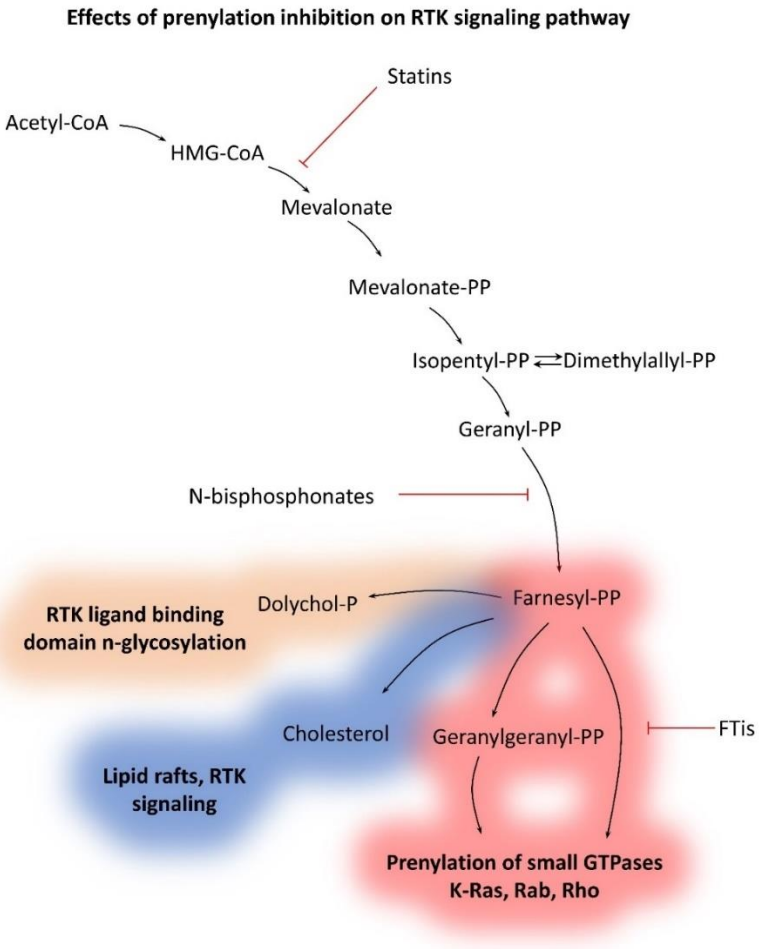

Figure 3 Effects of different classes of prenylation inhibitiors on receptor tyrosine kinase (RTK) related signaling. Statins and N-bisphosphonates block biosynthesis of farnesyl-PP, resulting in inhibition of prenylation and impoverishment of cholesterol and dolichols. Dolichols are required for N-glycosylation process that is necessary for certain RTKs, e.g. EGFR for functioning. Cholesterol is essential component of lipid rafts that function as center for numerous signaling cascades. Depletion of cholesterol results in altered signalization (e.g. EGFR and HER2). Inhibition of prenylation affects major cellular processes, involving vesicular transport and autophagy (RAB proteins) or proliferation, growth, survival or migration (KRAS, RHEB, RAL) [31]

Furthermore, in case of statins and bisphosphonates, metabolic inhibition of the mevalonate pathway bears other consequences besides blockade of prenylation (**Figure 3**). Squalene biosynthesis is rooted on the mevalonate pathway that affects synthesis of dolichols (functioning in protein glycosylation),steroid hormones like estrogens and - last but not least - cholesterol that is an essential component of lipid rafts [98].

Focusing to the intracellular level, depletion of cholesterol from lipid rafts radically changes plasma-membrane associated signalization, as lipid rafts (specific microdomains within the PM enriched with cholesterol) has been shown to be important centers of numerous distinct signaling pathways (**Figure 3**) [99].

EGFR has been shown to be localized in lipid rafts under physiological conditions [100]. Furthermore, blockade of lipid raft localization of HER2 inhibited breast cancer cell proliferation [101], and cholesterol depletion by lovastatin treatment eliminated resistance of breast cancer cells to EGFR inhibition [102].

Additionally, as mentioned above, upstream blockade of mevalonate pathway by statins and N-bisphosphonates also interfere with formation of dolichols that are involved in N-glycosylation. EGFR is a highly glycosylated protein and N-glycosylation is essential for its proper ligand binding [103]. Aberrant glycosylation of EGFR has been found in colorectal cancer specimens compared to vicinal normal tissue [104]. Interestingly, liver cells treated with statin have been shown to have altered glycosylation of surface proteins [105].

In summary, blockade of mevalonate pathway by statins and N-bisphosphonates may interfere with EGFR signaling by inhibiting lipid raft localization and blocking N-glycosylation (**Figure 3**).

2. Objectives

Aim of this dissertation was to investigate applicability and anticancer effects of various prenylation inhibitors on tumors harboring KRAS mutation. Special care was taken to carry out the experiments with a clinical perspective; e.g. using drugs that were tested in clinics or investigate drug settings that potentially avoid known side effects. Thus, our objectives were the following:

1) Compare anti-tumor effects of a recently established lipophilic bisphosphonate with the clinically approved zoledronate on cellular and xenograft model of colorectal cancer.
2) Investigate mutant KRAS specific effects of bisphosphonates.
3) Compare anticancer effects of different classes of prenylation inhibitors on different types of human tumors in regard to their *KRAS* mutational status.
4) Examine potential combinatorial strategies using KRAS G12C inhibitors and various prenylation inhibitors in human preclinical cancer models.

3. Methods

3.1 *In silico* analysis

In silico data were obtained from the publicly available www.depmap.org website using drug sensitivity data from the Repurposing Primary Screen [106]. This database contains sensitivity values of thousands of drugs at 2.5 μM concentration for 5 day-long treatments using 750 cell lines of various tissue of origins. We collected data for three distinct classes of prenylation inhibitors, namely statins, N-bisphosphonates and farnesyl-transferase inhibitors. Sensitivity values were grouped based on *RAS* mutational status using the https://depmap.org/portal/interactive/ tool and were also manually reviewed. Cells carrying *KRAS* hotspot mutations (G12, G13, Q61 mutations based on COSMIC and TCGA database) were compared to cell lines with wild type *RAS*. Drug-to-drug differences between drug classes were eliminated by combining data of all available drugs of the distinct classes together. List of drugs used for the analysis is shown in **Table 1**. Notably, for lung cancer only data of lung adenocarcinoma cells were used for tissue-specific analysis.

Table 1. List of drugs used for *KRAS* mutation dependent analysis of different classes of prenylation inhibitors.

Statins	N-bisphosphonates	FTis
Atorvastatin	Alendronate	Lonafarnib
Lovastatin	Pamidronate	Tipifarnib
Mevastatin	Ibandronate	
Pitavastatin	Neridronate	
Pravastatin		
Rosuvastatin		
Simvastatin		

3.2 Cells cultures

All cell lines used are listed in **Table 2** along with their histological classification, *KRAS*/*BRAF* mutational status (focusing mainly on RTK pathways) and references.

Table 2. List of cells used in this thesis. Histological classification, *BRAF*/*KRAS* mutational status and origin of cells are also indicated.

Cell line	Histology and origin	Mutational status	References
CACO2	colorectal adenocarcinoma	*KRAS* WT *BRAF* WT	ATCC
HCA7	colorectal adenocarcinoma	*KRAS* WT *BRAF* WT	ECACC.
WIDR	colorectal adenocarcinoma	*KRAS* WT *BRAF* V600E	ATCC
SW1417	colorectal adenocarcinoma	*KRAS* WT *BRAF* V600E	ATCC
SW480	colorectal adenocarcinoma	*KRAS* G12V *BRAF* WT	ATCC
DLD1	colorectal adenocarcinoma	*KRAS* G13D *BRAF* WT	ATCC
HCT116	colorectal adenocarcinoma	*KRAS* G13D *BRAF* WT	ATCC
DKO4	colorectal adenocarcinoma	*KRAS* WT *BRAF* WT	Knockout derivative of DLD1, kindly provided by Senji Shirasawa [107]
HKH2	colorectal adenocarcinoma	*KRAS* WT *BRAF* WT	Knockout derivative of HCT116, kindly provided by Senji Shirasawa [107]
H358	lung adenocarcinoma	*KRAS* G12C *BRAF* WT	ATCC
H1792	lung adenocarcinoma	*KRAS* G12C *BRAF* WT	ATCC
SW1573	lung adenocarcinoma	*KRAS* G12C *BRAF* WT	ATCC
PF139	lung adenocarcinoma	*KRAS* G12C *BRAF* WT	Developed by B Hegedűs from pleural effusion

Cells were cultured in DMEM (Lonza, Switzerland; with 4500 mg/dm3 glucose, pyruvate and L-glutamine Cat.no.: 12-604F) supplemented with 10% fetal calf serum (EuroClone; Cat.no.: ECS0180L) and 1% penicillin-streptomycin-amphotericin (Lonza; Cat.no.: 17745) in tissue culture flasks in a humidified 5% CO2 atmosphere at 37 ºC. In order to avoid mycoplasma infection, medium was supplemented with BM Cyclin (BMC) (Sigma; Cat.no.: 10799050001) alternating BMC1 and BMC2 every third day. BMC was not applied during the experiments.

Drugs were dissolved in DMSO at 5 or 10 mM concentration and were kept on -80 °C aliquoted except for drugs used in combinational *in vivo* experiments, which is detailed in the appropriate section.

Table 3. List of drugs used in this thesis for *in vitro* and *in vivo* experiments.

Name	Drug type	Source
Zoledronate	N-bisphosphonate	Novartis
BPH1222	N-bisphosphonate	[108]
Simvastatin	statin	Sigma; Cat.no.: S6196
Lonafarnib	FTi	Sigma; Cat.no.: SML1457
Tipifarnib	FTi	Sigma Cat.no.: SML1668 (*in vitro*), Medchemexpress; Cat.no.: HY-10502 (*in vivo*)
ARS1620	KRAS G12C inhibitor	Medchemexpress; Cat.no.: HY-U00418
AMG510	KRAS G12C inhibitor	Medchemexpress; Cat.no: HY-114277

3.3 Clonogenic assay

Clonogenic assay was used for determination of long-term effects of ZA and BPH1222 (also used later as BPH) on cellular proliferation and clonogenic potential. In brief, cells were plated in 1000 cells/well density to 6-well plates and treated with 1 and 2 μM ZA or BPH1222 from the following day for 8 days. Medium was changed on every 3rd day. Plates were washed and attached cells fixed on the 8th day with mix of methanol and acetic acid (3:1 ratio) for half an hour at room temperature. Fixed cells were then stained with crystal violet. Excess die was washed with dH_2O and cell-bound die was dissolved

in 2% SDS and measured at 570 nm with a microplate reader (EL800, BioTec Instruments, Winooski, VT).

3.4 2D combinational tests

Cells that reached 70-80% confluency were trypsinized and counted using Luna II Automated Cell Counter. Cells were plated in 5000-10000 cells/well density (depending on the growth rate of the given cell line) on a 24-well plate. Next day the medium was replaced to fresh medium supplemented with different concentrations and combinations of the inhibitors. After 6 days, the wells were washed with DPBS (Lonza; Cat.no.: 17-512F) and the cells were fixed by 10% trichloroacetic acid for 1 hour at 4 °C and then stained with Sulforodamine-B (SRB) (Sigma; Cat.no: S1402) dye for 15 minutes. Plates then were repeatedly washed with 1% acetic acid to remove excess dye. Protein-bound SRB was then dissolved in 10 mM Tris buffer (pH=7.4) and OD was measured at 570 nm using a microplate reader (EL800, BioTec Instruments, Winooski, VT). OD values were normalized to control and these data then were used to calculate combinational index (CI) values using Compusyn software as described in [109]. Briefly, the combinational index theorem was introduced to model combinational drug interactions. CI values are used to the characterization of these interactions; CI values less than 1 indicate synergy while values equal to or more than 1 represent additive or antagonistic effect, respectively. Data shown are results of three independent experiments.

3.5 3D spheroid clonogenic assay

For earlier experiments utilizing spheroids for long-term bisphosphonate treatment, hanging drop method was used. Spheroids were generated in 6 µl drops (each containing approximately 300 or 700 cells depending on cell line. Spheroids were formed in 3 or 4 days of incubation and were then transferred to the inner 60 wells of a 96-well Ultra Low Attachment Plate (VWR; Cat.no.: 29443-034), only one spheroid to each well. Spheroids were then treated with 2 and 5 µM ZA and BPH1222 for 12 days. Spheroids were photographed using a ToupCam XW 3MP microscope-camera on the first day, and every 3rd day throughout treatment. Medium was also changed partially on every 3rd day: 90 µl medium was replaced to 100 µl of fresh medium (in order to compensate evaporation). Data shows at least ten spheroids from three independent experiments.

3.6 3D spheroid combinational tests

As 3D environment models more accurately *in vivo KRAS* dependency, combination studies were investigated also using multicellular tumor spheroids. Spheroids were generated using polyHEMA (Sigma; Cat.no.: P3932) coated 96-well round bottom plates (Sarstedt; 833925500). Briefly, the inner 60 wells of the plate were coated with 60 µl 5 mg/ml polyHEMA dissolved in 96% ethanol. Plates were dried at 60 °C in a plate shaker while shaking, then sterilized with UV for half an hour. Cells were seeded at 3000 cells/well density at the inner 60 polyHEMA coated wells in 200 µl medium, while the outer wells were filled with DPBS to avoid evaporation. Plates were then centrifugated at 2000 RPM so that cells would be concentrated at the bottom of the well thus enhancing single spheroid formation. Within 24 hours the cells aggregated into spheroids and were treated by adding further 100 µl medium supplemented with different concentrations and combinations of the inhibitors. Each concentration group contained three spheroids. Each spheroid was photographed using a ToupCam XW 3MP microscope-camera on the first and sixth day of the treatment.

3.7 3D image analysis

Before imaging, medium was gently suspended so that unattached or dead cells would be removed from the surface of the spheroids. Images then were analyzed using ImageJ software with a modified script of [110]. Briefly, the script measures the area of the 2D projections of the spheroids. Results were manually reviewed, then area values were used to calculate radius and volume of spheroids using the formula $V=4/3 \times \pi \times radius^3$. Data are shown as results of three independent experiments.

3.8 Cell cycle experiments

Determination of DNA content in each cell using NucleoCounter NC-3000™ system (Chemometec) was used to evaluate the number of cells in each cell cycle phase as described earlier [111]. 500 nM Tipifarnib, 100 nM AMG-510 and their combination were used for treatment. All cells were treated for 96 hours in 6-well plates, except for H358, which was only treated for 48 hours due to its higher sensitivity to AMG510. Following treatment, samples were prepared using kit of the system according to the manufacturer's instructions. Cells were trypsinized and lysed before staining with DAPI for 5 min at 37°C. Then, after adding the stabilization buffer 10 µl of each sample was

loaded onto an 8-well NC slide. NucleoCounter NC-3000™ system (Chemometec) was used to quantify cellular fluorescence.

3.9 Western blot

Cell signaling was investigated by western blot analysis. Following 48 hours treatment with 500 nM Tipifarnib, 100 nM AMG510 and their combination in 6-well plates, cells were washed with DPBS and fixed with 6% trichloroacetic acid for an hour at 4°C. Cells then were mechanically harvested and centrifuged. Precipitated protein was dissolved in modified Läemmli-type sample buffer containing 0.02% bromophenol blue, 10% glycerol, 2% SDS, 100 mM dithiothreitol (DTT), 5 mM EDTA, 125 mg/ml urea, 90 mM Tris-HCl, pH 7.9. Qubit Fluorometer was used for determination of Protein concentration. Equal amounts of protein were loaded onto 10% polyacrylamide gels and transferred after electrophoretic separation to PVDF (Thermo Fisher; Cat.no.: 88520) membranes. Analysis of KRAS signaling were performed using KRAS4B (Sigma; Cat.no.: WH0003845M1), p-AKT (Cell Signaling; Cat.no.: 4058S,), AKT (Cell Signaling; Cat.no.: 9272S), p-S6 (Cell Signaling; Cat.no.: 2215S), S6 (Cell Signaling; Cat.no.: 2217S), p-ERK (Cell Signaling; Cat.no.: 9101S), ERK (Cell Signaling; Cat.no.: 9102S) primary antibodies. RHEB antibody (Cell Signaling; Cat.no.: 13879S) was used for evaluation of farnesyl-transferase inhibition. For detection of apoptosis PARP (Cell Signaling; Cat.no.: 9545S) primary antibody was used. PCNA (Cell Signaling; Cat.no.: 13110S) primary antibody was used for detection of proliferation. B-TUBULIN antibody was purchased from Cell Signaling (Cat.no.: 2128) All antibodies were dissolved according to the manufacturer instructions in 5% BSA or dry milk in 1x TTBS buffer. Membranes were blocked at room temperature in 5% dry milk dissolved in 1x TTBS for an hour, then were incubated in primary antibodies overnight at 4°C. HRP conjugated anti-rabbit secondary antibodies (1:10000, 1 h, RT) and Pierce ECL Western Blotting Substrate (Kvalitex; Cat.no.: EMP001005) were used for visualization. Ponceau staining (Sigma; Cat.no.: P3504) was used for normalization. Quantification was performed using ImageJ software. Each cell lines were analyzed in 3 biological replicates.

3.10 Videomicroscopic analysis

For videomicroscopic analysis, SW1573 cells were seeded on a 24 well plate at 5000 cells/well densitiy. Next day the medium was replaced to fresh medium supplemented

with tipifarnib (500 nM) or AMG510 (100 nM) or combinational treatment. Each treatment group involved three independent wells. Images were taken from one field of view of each wells in every 10 minutes for 72 hours using ZenCellowl incubator microscope (innoME). Mitotic activity of SW1573 cells were counted using Cell Counter plugin of the ImageJ Fiji software. Briefly, 350000 point per area (pixels^2) were applied to the videos, then three pre-determined squares were manually reviewed, and cell mitosis was counted using Cell Counter plugin. Number of cell divisions of each field of view were summed from 0 to 24th, from 24th to 48th and finally from 48th to 72nd hours of the experiments. Each graph shows combined results of three independent experiments.

3.11 *In vivo* experiments

For bisphosphonate experiments, SW1417 and HCT116 human colorectal cancer cells (5 × 10^6 and 3 × 10^6 in 0.2 ml serum-free DMEM, respectively) were injected subcutaneously into the flank of male SCID mice. Tumors were already quantifiable 4 days following injection and animals were randomized and assigned according to treatment conditions (control, ZA and BPH1222 treated), each group containing 10 animals. Treatment started after 4 and 8 days after injection in case of HCT116 and SW1417 xenografts, respectively. In order to make sure that the inhibitors are injected in equal amounts/kg, we decided to treat with equimolar doses instead of equal mass/kg. Thus, mice were treated with 1.47 μmol/kg ZA or BPH1222 dissolved in steril DPBS intraperitoneally twice a week for 3 weeks. As BPH1222 is the modified version of ZA, it has a significantly higher molar massControls were injected with 100 μl of 0.9% sodium-chloride solution. Tumors were measured with caliper and volumes were calculated using formula for the volume of a prolate ellipsoid ($4/3\pi$ × (length ×width^2). Three animals from each group were sacrificed from the HCT116 experiment on the 14th day of treatment for monitoring drug effects by histological investigation (data not shown). Last measurement was performed on day 21, and all remaining mice (7 in each group) were sacrificed by cervical dislocation. As SW1417 xenografts exhibited rapid growth rate, the experiment had to be terminated on the 15th day of the treatment.

For combinational experiments, H358 and SW1573 human lung adenocarcinoma cells (5×10^6 and $1x10^6$, respectively) were subcutaneously injected in female SCID mice. Cells were injected in 200 μl DMEM:Matrigel (VWR; Cat.no.: 734-0273) mixture (ratio 1:1) based on preliminary experiments. When tumor reached approximately 100 mm^3 (H358

7 days, SW1573 26 days after injection), animals were randomized and treated intraperitoneally daily except for weekends. Drugs were dissolved in 60% DPBS, 34% PEG300 (Sigma; Cat.no.: 90878), 5% DMSO and 1% Tween80 (Sigma; Cat.no.:P1754). H358 xenografts were treated with 5 mg/kg AMG510; 40 mg/kg Tipifarnib, while SW1573 xenografts were treated with 25 mg/kg AMG510 and 40 mg/kg Tipifarnib. Controls received vehicle. The subcutaneous tumors were measured with a caliper and tumor volumes were calculated with the formula $V=4/3\pi \times (\text{length} \times \text{width}^2)$ and expressed in mm^3. H358 experiment was terminated after 18 days and SW1573 after 25 days treatment. Tumors were measured upon harvest, then fixed with 4% PFA for histological analysis (data not shown).

Animals were the properties of the Department of Experimental Pharmacology, National Institute of Oncology, H-1122, Budapest, Hungary. All experiments were carried out in accordance with the Guidelines for Animal Experiments and were approved for the Department of Experimental Pharmacology in the National Institute of Oncology, Budapest, Hungary (permission number: PEI/ 001/2574–6/2015).

3.12 Statistics

Kolmogorov-Smirnov normality test was used for confirmation of normal distribution of dependent variables. Statistical differences between groups were determined using repeated measures ANOVA for spheroid data and xenograft experiments in ZA and BPH1222 experiments. All ANOVA tests with significant differences were followed by Bonferroni's post hoc test. Mann-Whitney U test was applied for clonogenic assay using DLD1 and HCT116 and their knockout derivatives. Otherwise, non-parametric Kruskal-Wallis and post hoc Dunn's multiple comparison test was used in clonogenic assays and cell cycle experiments. "*In silico*" data derived from PRISM Repurposing Primary Screen were analyzed by two-tailed t-test. In case of *in vivo* FTi and AMG510 combinational experiments, unequal numbers due to animal losses during the experiments prevented use of repeated measures ANOVA or mixed ANOVA. Instead, last day's relative tumor growth data were tested with non-parametric Kruskal-Wallis and post hoc Dunn's multiple comparison test. Regarding tumor mass, one-way ANOVA was used for testing SW1573 tumors, while due to lack of normal distribution, non-parametric Kruskal-Wallis and post hoc Dunn's multiple comparison test was used for H358 tumors. Statistical

significance was established at $p < 0.05$. All statistical analysis were computed by GraphPad Prism 5 (GraphPad Software Inc, USA, San Diego, CA).

4. Results

4.1 Effects of long-term treatment with bisphosphonate drugs on monolayer cultures

Long-term effects of ZA or BPH1222 treatment was investigated by clonogenic assay (**Figure 4**). No significant difference could be determined in sensitivity to bisphosphonates based on major oncogenic mutations. Statistical significance could only be observed in case of HCA7 cells both at 1 μM and 2 μM concentrations where ZA exhibited more robust inhibition on clonogenic growth compared to BPH1222, whereas BPH1222 was significantly more effective in SW480 cells at 1 μM concentration. Higher efficacy of BPH1222 compared to ZA at inhibition of HCT116 cells did not reach significance though they could be considered to be at biological relevance.

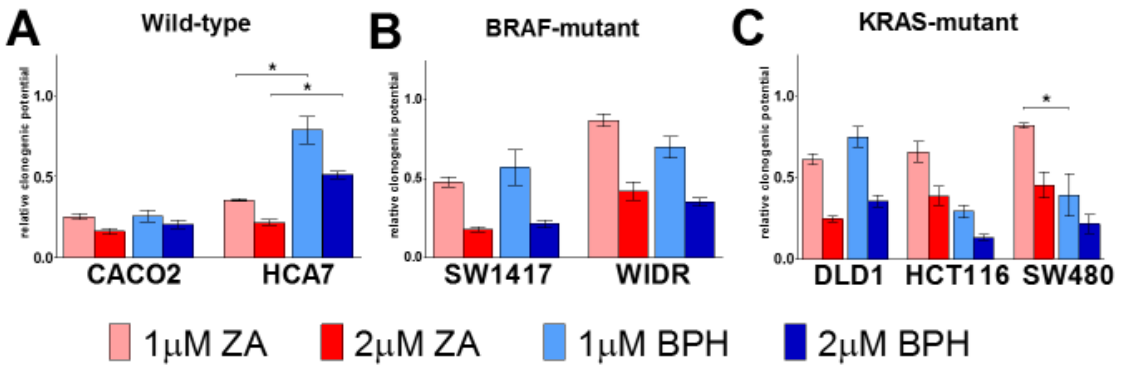

Figure 4 Results of bisphosphonate treatment on clonogenic potential of colorectal cancer cells. a) CACO2 and HCA7 (*BRAF*, *KRAS* wild-type), b) SW1417, WIDR (*BRAF* mutant), c) DLD1, HCT116, SW480 cells (*KRAS* mutant). Drugs exerted dose-dependent inhibition of clonogenic growth in all cell lines independently from mutational status. Data are depicted as relative to control showing average ± SEM of three independent experiments. Significant differences between ZA and BPH1222 with $p < 0.05$ are indicated with asterisks. Statistical analysis were carried out using non-parametric Kruskal-Wallis followed by post hoc Dunn's multiple comparison test [108].

4.2 Effects of bisphosphonate treatments on cell cycle of colorectal cancer cells

In vitro changes of cell cycle distribution upon ZA or BPH1222 treatment was determined by DAPI staining and image cytometry (**Figure 5)**. Both drugs increased proportion of S-phase as well as subG1-phase (apoptotic) cells in *KRAS* and *BRAF* wild type CACO2 and *BRAF* V600E mutant WIDR cells. At the same time, robust reduction of ratio of G0/G1 phase cells could be observed. Of note, BPH1222 treatment resulted in more pronounced

changes, as increase in S-phase was significantly higher in WIDR cells at both concentrations of BPH1222 and upon 10 μM treatment in CACO2 cells compared to control. 10 μM BPH1222 treatment induced also significant increase of subG1-phase in CACO2 cells. Interestingly, bisphosphonate treatment of *KRAS* mutant HCT116 cells exerted only minimal effects in cell cycle distribution, as only a slight – but significant - increase in the ratio of subG1 phase could be observed upon BPH1222 treatment. ZA treatment was able to induce significant changes in none of the cell lines investigated.

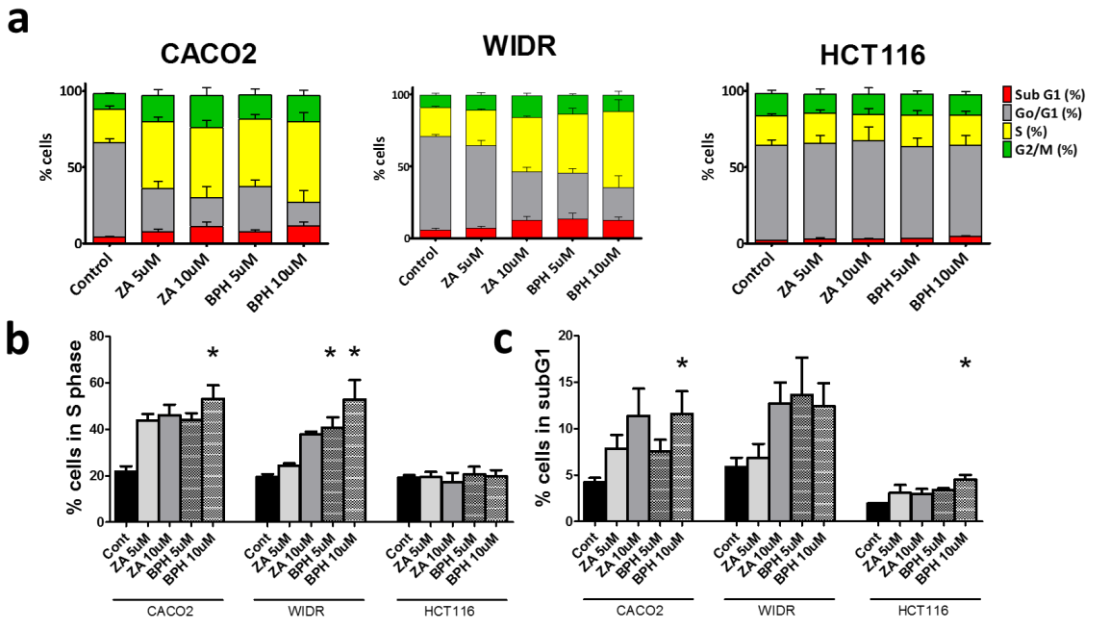

Figure 5 Investigation of effects of 72-hour treatment with ZA and BPH1222 on cell cycle of colorectal cancer cells. **(a-c)** show changes in cell cycle distribution upon treatment in CACO2, WIDR and HCT116 cells. Increase of S-phase **b)** and subG1-phase cells **c)** following ZA or BPH1222 exposure. Both drugs resulted in increased S- and subG1-phase in CACO2 (BRAF, *KRAS* wild-type) and WIDR (*BRAF* V600E mutant) cells. Only a slight increase in subG1-phase cell could be observed in HCT116 (*KRAS*-mutant) cells. Data are shown as average ± SEM of three independent experiments for each cell line. Significant differences between control and bisphosphonate treatment with $p < 0.05$ are indicated with asterisks. Statistical analysis were carried out using non-parametric Kruskal-Wallis followed by post hoc Dunn's multiple comparison test[108].

4.3 Effects of bisphosphonates on KRAS signaling and induction of apoptosis

Distinct changes could be observed upon 48-hours-long *in vitro* treatment with ZA and BPH1222 on PI3K/AKT and RAF/MEK/ERK cascades, two major signaling pathways regulated by KRAS (**Figure 6**). Bisphosphonate treatment elevated p-ERK level in all three colorectal cancer cell lines carrying *KRAS* mutation as well as in and *BRAF* V600E mutant SW1417. Interestingly, the other *BRAF* V600E mutant WIDR and *BRAF*, *KRAS*

wild type CACO2 and HCA7 cell lines showed no biologically relevant change in the level of phosphorylated ERK protein. Level of p-S6 (marking activation of PI3K/AKT/mTOR signaling) decreased robustly in all cell lines with the exception of SW1417 (*BRAF* V600E mutant), where apparently a small increase could be observed in S6 activation. Notably, observed effects (increase or reduction in the activation of ERK or S6) were more pronounced in general upon BPH1222 treatment. Furthermore, both bisphosphonate induced apoptosis based on the detection of cleaved PARP in CACO2, HCA7 and HCT116 cell lines.

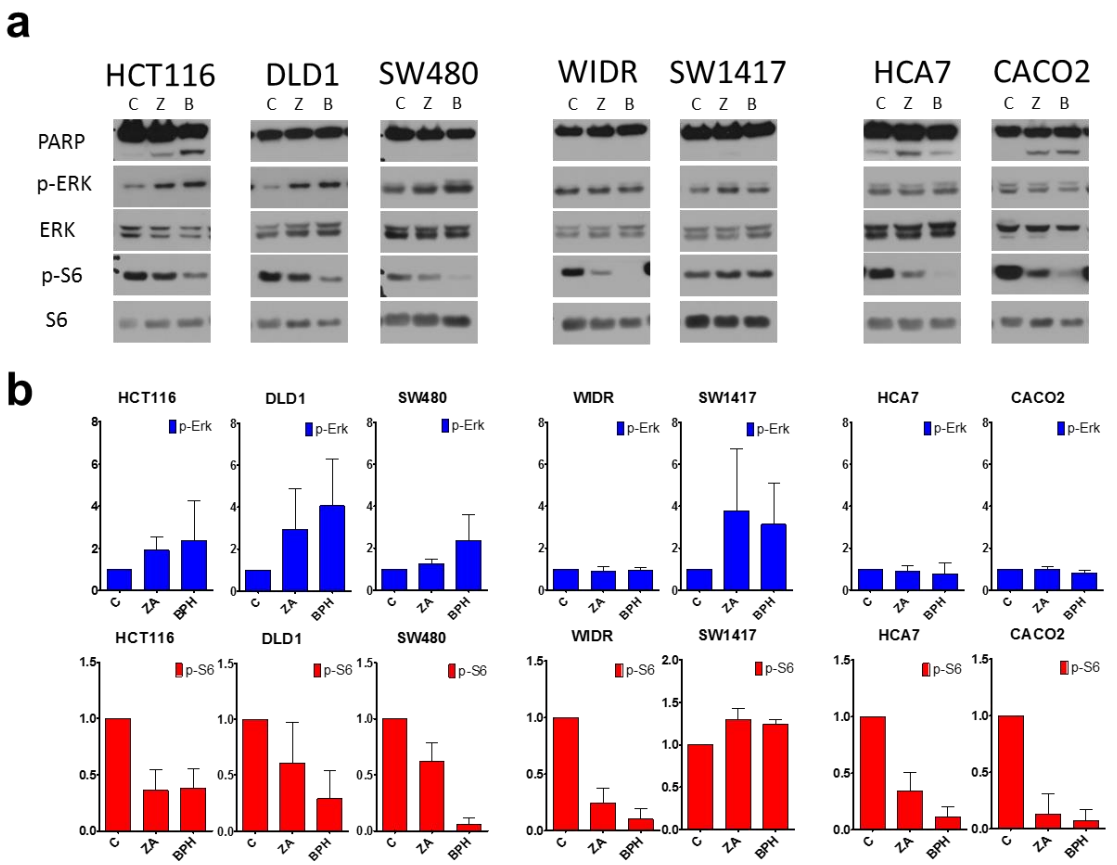

Figure 6 Effects of 48-hour-long treatment with 10 μM ZA or BPH1222 on KRAS related cell signaling in colorectal cells. a) Shows representative blots of proteins investigated, b) shows effects of treatment on activation level of ERK and S6. Protein levels were normalized to total protein (using Ponceau staining, data not shown) and to control. Cleaved PARP indicates apoptosis induction in HCT116, HCA7 and CACO2 cells upon bisphosphonate treatment. BPH1222 was more effective in apoptosis induction in HCT116 cells while ZA induced apoptosis more effectively in HCA7. p-ERK increased in *KRAS* mutant HCT116, DLD1 and SW480 cells as well as in *BRAF* mutant SW1417 cells. Bisphosphonate treatment reduced robustly activation of S6 in all cell lines with the exception of SW1417 where a small increase in p-S6 could be observed upon treatment. Data are shown as average ± SD of three independent experiments for each cell line [108].

4.4 Effects of bisphosphonate treatment on spheroid cell culture

Inhibitory effects of ZA and BPH1222 treatment on spheroid growth are shown in **Figure 7**. Four of the seven investigated cell lines were capable of sphere formation: *KRAS* G13D mutant DLD1 and HCT116 and two *BRAF* V600E mutant SW1417 and WIDR. Of importance, lipophilic BPH1222 was more effective in blocking spheroid growth compared to ZA. Inhibitory effects of bisphosphonates were not dependent on *KRAS*/*BRAF* mutational status.

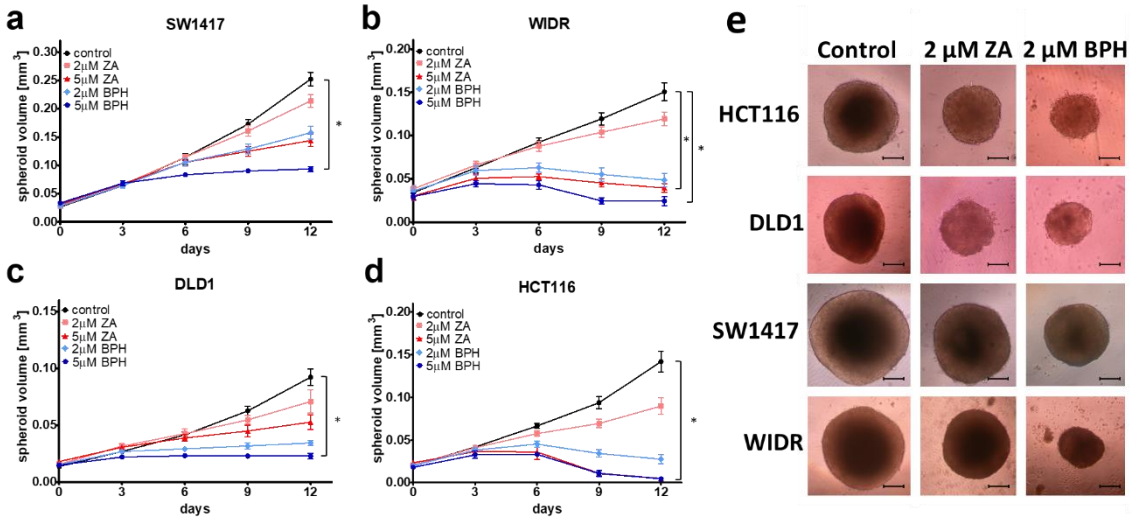

Figure 7 Inhibitory effects of 12-day-long ZA or BPH1222 exposure on spheroid growth. (a-d) Volume of spheroid was calculated based on pictures taken on every third day (details in Methods). e) Representative images of spheroids at the last day of the experiment (2 µM concentration ZA or BPH1222). Scale bar=200 µm. BPH1222 showed higher inhibitory effect on spheroid growth. Data are shown as average ± SEM of at least ten spheroids for each cell line from three independent experiments. Significant differences are indicated by asterisks ($p < 0.05$ compared to control). Statistical significance was calculated with repeated measures ANOVA and Bonferroni post hoc tests [108].

4.5 *In vivo* effect of bisphosphonate treatment

To validate *in vitro* findings on the effect of bisphosphonate treatment in *in vitro* settings, HCT116 (*KRAS* G13D mutant) and SW1417 (*BRAF* V600E mutant) subcutaneous xenograft models were established in male SCID mice. Both drugs decreased the growth of HCT116 xenografts, however, only BPH1222 treatment exerted significant inhibitory effects compared to control **(Figure 8a)**. In contrast with these results, SW1417

xenografts proved to be highly resistant to both bisphosphonates *in vivo*, and both treatments failed to inhibit growth of the subcutaneous tumors **(Figure 8b).**

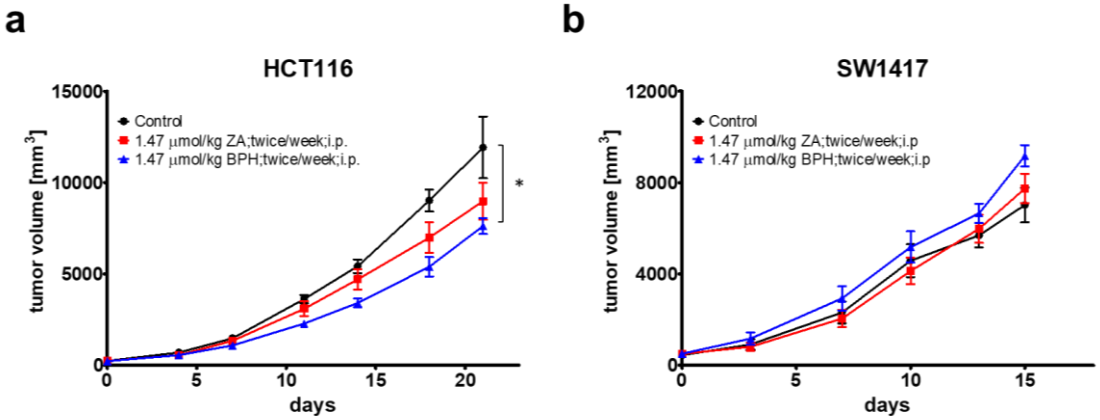

Figure 8 *In vivo* subcutaneous xenograft experiment using human colorectal cancer cells. a) HCT116 (*KRAS* G13D mutant) and b) SW1417 (*BRAF* V600E mutant) xenograft tumor growth treated with 1.47 mol/kg (equimolar) ZA and BPH1222. Data are shown as average of ten tumors/group ± SEM. Significant difference (indicated with asterisk) was established at $p < 0.05$ and was tested repeated measures ANOVA and Bonferroni post hoc tests [108].

4.6 Investigation of effects of bisphosphonate treatment upon knockout of the mutant KRAS allele

In order to investigate mutant KRAS dependent effects of bisphosphonate treatment, clonogenic assay was performed using isogeneic cell derivatives of *KRAS* G13D mutant cell lines. DKO4 (-/WT) was generated from DLD1 (*KRAS* G13D/WT) while HKh-2 (-/WT) originates from HCT116 (*KRAS* G13D/WT). **(Figure 9a-b).** Interestingly, disruption of the mutant *KRAS* allele resulted in increased sensitivity to BPH1222 treatment in DKO-4 (-/WT) cells compared to DLD1 (G13D/WT) cells. By contrast, HKh-2 (-/WT) cells apparently became more resistant to BPH1222 treatment compared to its parental cell line HCT116 (G13D/WT) while we could not observe differences in sensitivity to ZA treatment between parental and knockout cells. Analysis of cell signaling also revealed differences in response to bisphosphonate treatment between parental and knockout lines (**Figure 9b-c**). Interestingly, drug induced strong activation of ERK in DLD1 and HCT116 (*KRAS* G13D/WT) was abolished in the knockout clones (-/WT). Notably, pattern of ERK activation in HKh-2 showed similarity to *BRAF*, *KRAS* double wild-type cell lines CACO2 and HCA7. Furthermore, bisphosphonate treatment

failed to induce apoptosis (based on level of cleaved PARP) in HKh-2 (-/WT) in contrast with its parental line HCT116 (G13D/WT).

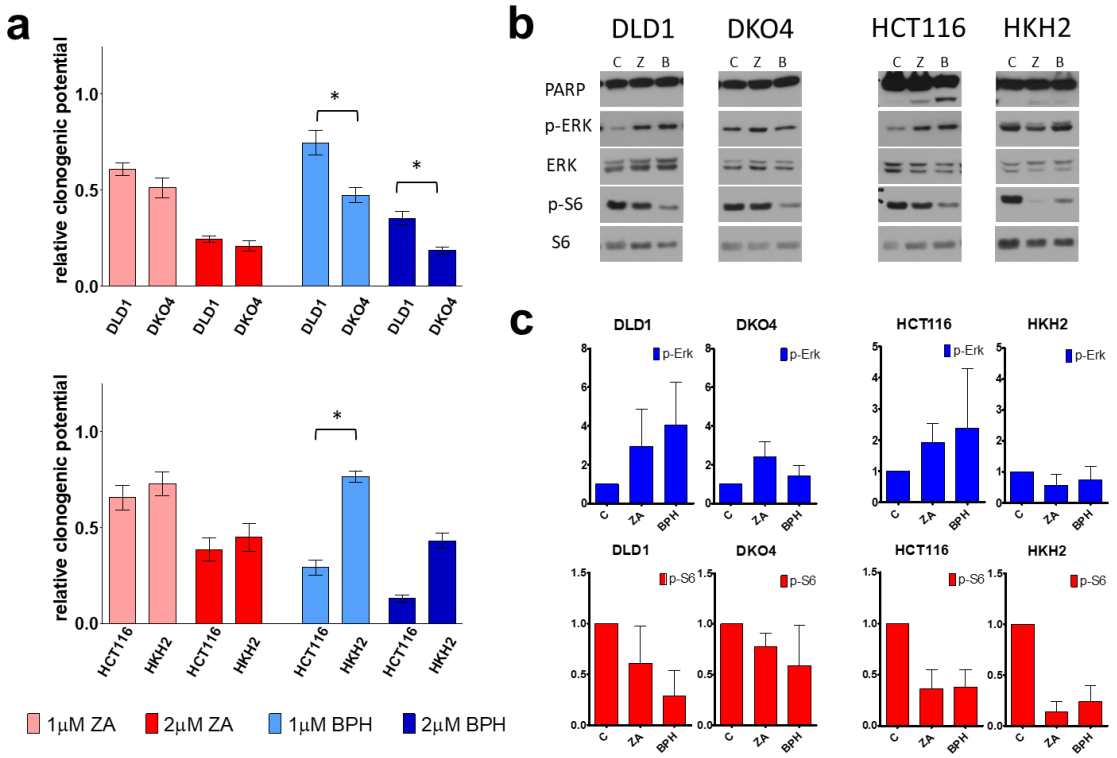

Figure 9 Investigation of the role of mutant KRAS allele in response to prenylation inhibition. Both DLD1 and HCT116 harbor heterozygous *KRAS* G13D mutations (G13D/WT). Mutant *KRAS* G13D allele was disrupted resulting in DKO-4 and HKh-2 (-/WT) cells. DKO-4 is the knockout derivative of DLD1, while HKh-2 originates from HCT116. a) Shows effects of long-term bisphosphonate exposure on parental and knockout lines. Differences could be observed only upon BPH1222 treatment that showed opposite effects in the parental and knockout pairs. DKO-4 (-/WT) was more sensitive to BPH1222 compared to DLD1 (G13D/WT), while HKh-2 (-/WT) apparently became more resistant to it compared to HCT116 (G13D/WT). Statistical significance was tested with non-parametric Mann-Whitney U test. (b-c) Show changes in cell signaling. Increased activation of ERK only could be observed in parental lines (G13D/WT) but not in knockout clones (-/WT). Disruption of *KRAS* G13D allele in HKh-2 abolished drug-induced apoptosis that could be observed in HCT116 (G13D/WT) [108].

4.7 *In silico* analysis

In order to asses broader spectrum of effects of prenylation inhibition and its association with *KRAS* mutation, we performed an "*in silico*" analysis using publicly available data from the PRISM Repurposing Primary Screen [106] on depmap.org. This screen contains sensitivity data of hundreds of cells in response to thousands of compounds. Data explorer

tool of depmap.org allows easy comparison of drug sensitivity data based on various cellular characteristics (e.g. tissue of origin, mutational data) derived from other high-throughput datasets. Accordingly, we compared sensitivity of *KRAS* mutant and wild type lung and colorectal adenocarcinoma cells using three classes of these prenylation inhibitory drugs, namely statins, N-bisphosphonates and farnesyl-transferase inhibitors (**Figure 10**). Interestingly, tissue specific sensitivity patterns emerged to the distinct prenylation inhibitor classes, however, differences only reached significance in lung adenocarcinoma. Colorectal cancer cells lines harboring *KRAS* mutation was found to be more resistant to N-bisphosphonates (p=0.12) and farnesyl-transferase inhibitors (p=0.17) compared to cells with wild type *RAS* genes. Lung adenocarcinomas apparently show opposite behavior: N-bisphosphonates and FTi-s block cells with *KRAS* mutations more effectively than wild type cells (p=0.136 and p=0.007, respectively). No significant differences could be established analyzing statins (p>0.5).

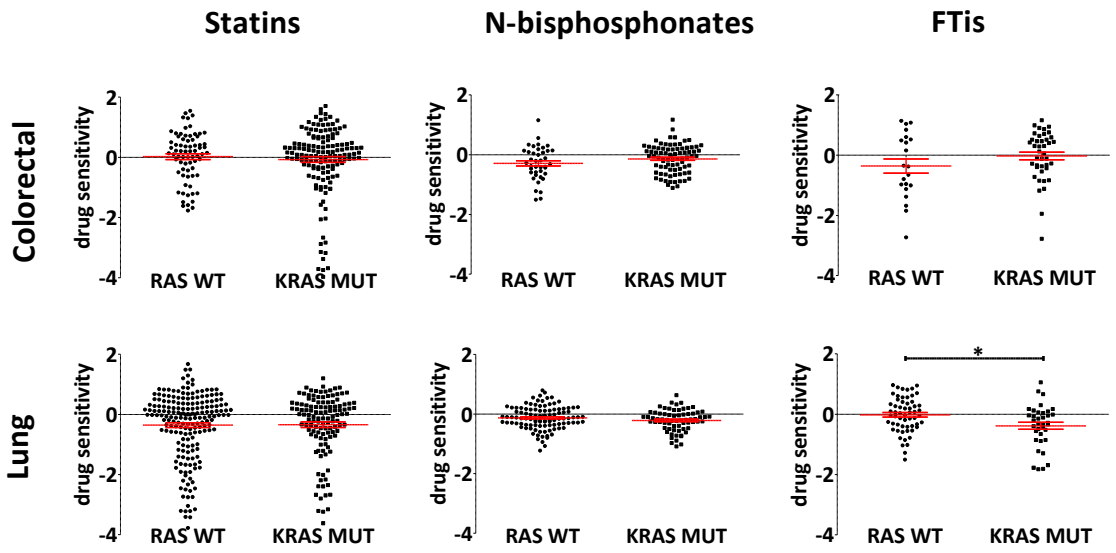

Figure 10 Drug sensitivity values of lung and colorectal adenocarcinoma cells. Data derives from PRISM Repurposing Primary Screen [106]. Inhibitory effects of statins, N-bisphosphonates and farnesyl-transferase inhibitors comparing cells with *KRAS* mutations to those with wild type *RAS*. List of drugs used are listed in **Table 1**. Significant difference could only be observed in FTi-treated lung cancer cells (two—tailed t-test, p<0.05). Interestingly, opposite trends could be observed in response to N-bisphosphonate and farnesyl-transferase inhibitors between colorectal and lung cancer cells. Analysis contains for CRC lines: *RAS* WT n~10; *KRAS* MUT n~20; for LUAD: *RAS* WT n~28; *KRAS* MUT n~18. A small variation can be found between the amount of cells with available data for the drugs included in the analysis [31].

4.8 2D combinational tests

KRAS mutation dependent significant differences in response to FTi treatment in lung cancer cells lead us to question whether farnesyl-transferase inhibitors could enhance efficacy of recently approved KRAS G12C inhibitors. Thus, 2D growth inhibition assays were performed with single agents or in combination of AMG510 and tipifarnib on a panel of *KRAS* G12C mutant LUAD cell lines (**Figure 11**).

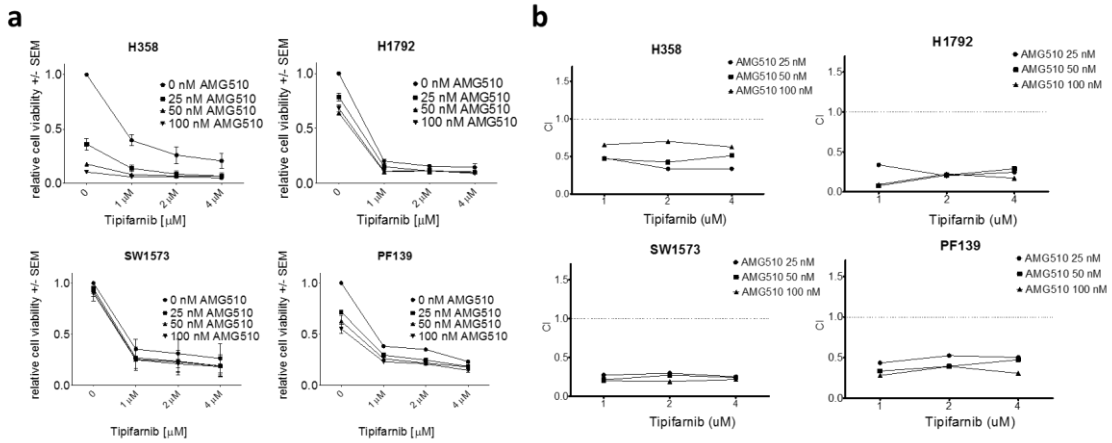

Figure 11 2D Growth inhibition assay with single agent or combination of AMG510 and tipifarnib. **a** Cell lines were treated with different concentrations of AMG510 or tipifarnib or both for six days. Relative cell viability is shown (mean, SEM, N). **b** Combination indexes of AMG510 and tipifarnib combinational treatment. Combination indexes (CI) were calculated by CompuSyn Software from the data of viability assays (A) of AMG510 and tipifarnib combination treatment. CI values less than 1 indicate synergy while values equal to or more than 1 represent additive or antagonistic effect, respectively.

Of note, tipifarnib was able to exert dose-dependent inhibition of all *KRAS* G12C mutant cell lines, in accordance with our *in silico* results. The growth inhibitory effect of tipifarnib was similar among the cell lines, except H1792, which was more sensitive compared to the other cells. H358 cell line was the most sensitive while H1792 and PF139 showed intermediate sensitivity and SW1573 was resistant to AMG510 treatment (**Figure 11/a**). Combination indexes (CI) were calculated by CompuSyn Software from the data of viability assays of combination treatment (**Figure 11/b**). All cell lines showed much lower CI value than 1 indicating strong synergistic interaction in combinational treatment. Synergism was also confirmed if other type of FTi (lonafarnib) or KRAS G12C mutant specific inhibitor (ARS-1620) was applied (**Figure 12**).

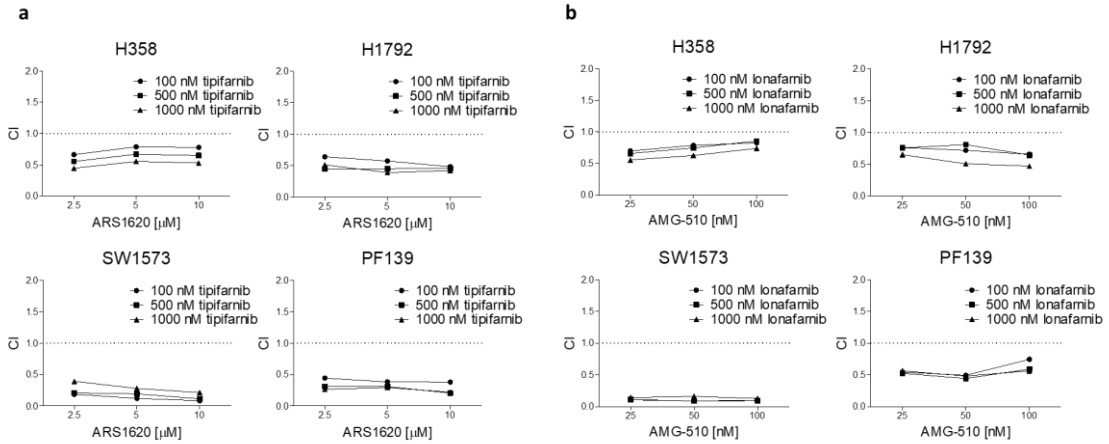

Figure 12 Growth inhibition assay with single agent or combination of ARS1620 and tipifarnib or AMG510 and lonafarnib. **A** Combination indexes of AMG510 and tipifarnib combinational treatment. Combination indexes (CI) were calculated by CompuSyn Software from the data of viability assays (data not shown) of ARS1620 and tipifarnib combination treatment **B** Combination indexes of AMG510 and lonafarnib combinational treatment. Combination indexes (CI) were calculated by CompuSyn Software from the data of viability assays (data not shown) of AMG510 and tipifarnib combination treatment. CI values less than 1 indicate synergy while values equal to or more than 1 represent additive or antagonistic effect, respectively.

4.9 3D spheroid combinational tests

3D growth inhibition assays were also performed with single agents or a combination of AMG510 and tipifarnib on our panel of *KRAS* G12C mutant LUAD cell lines to further confirm synergism (**Figure 13-14**).

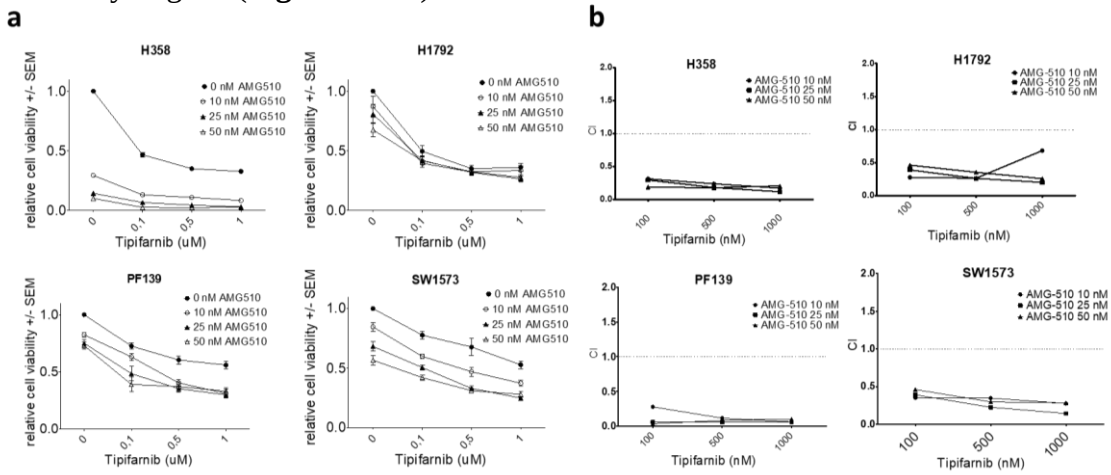

Figure 13 3D spheroid growth experiment of AMG510 and tipifarnib combination treatment. Spheroid volume was detected by taking pictures at the end of the experiment. **a)** Spheroids were treated with different concentrations of AMG510 or tipifarnib or both for six days. Relative cell viability based on spheroid volume assessment is shown on day 6 (mean, SEM). **b)** Combination indexes (CI) of AMG510 and tipifarnib combinational treatment. CI were calculated by CompuSyn Software from the data of viability assays of AMG510 and tipifarnib combination treatment (**a**). CI values less than 1 indicate synergy while values equal to or more than 1 represent additive or antagonistic effect, respectively.

Drug sensitivity to AMG510 and Tipifarnib was similar to 2D effects in most of the cell lines, only SW1573 showed higher sensitivity to AMG510 in 3D compared to 2D settings. This result is in accordance with published literature showing that KRAS dependence is more pronounced in 3D conditions [112]. Most importantly, CI values represented strong synergism similar to 2D results in all cell lines tested.

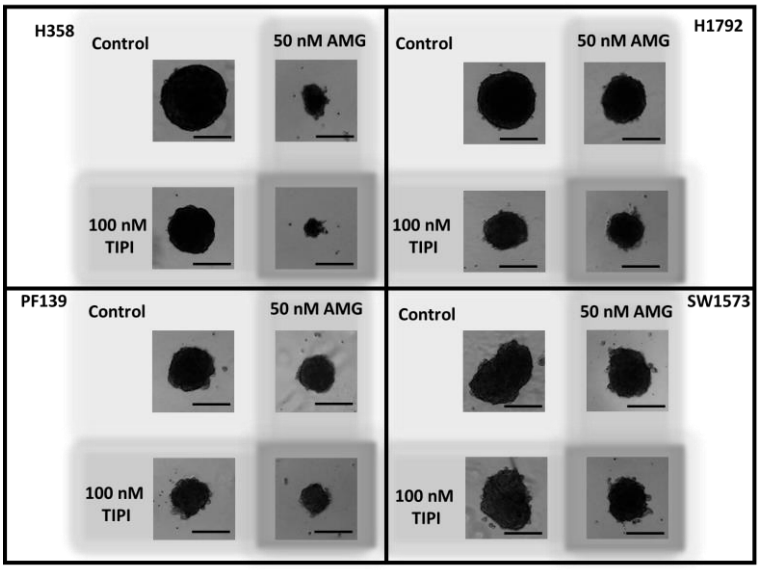

Figure 14 Representative pictures show the effect of the inhibitors on LUAD spheroids on the sixth day after treatment. Scale bar means 200 μm.

4.10 *In vivo* experiments testing FTi and KRAS G12Ci combinational therapy

We examined the effect of AMG510, tipifarnib or combined treatment on *in vivo* growth of H358 and SW1573 cells transplanted subcutaneously into female SCID mice (**Figure 15-16**). Notably, H358 was shown to be highly sensitive to AMG510 treatment, while SW1573 was resistant in 2D *in vitro* experiments. Thus, AMG510 dosage differed accordingly. Tipifarnib monotherapy resulted in strong tumor inhibition in the SW1573 tumor carrying homozygous mutant *KRAS* while AMG510 monotherapy could efficiently inhibit tumors of both cell lines. Relative growth values of tumors treated with AMG510 at the last day were found to be significantly smaller compared to control in SW1573 model (**Figure 15-16**) More importantly, combinational treatment resulted in the most pronounced inhibition of tumor growth, as demonstrated by either the tumor volume values measured during the experiment and the tumor weight values that was measured after termination (**Figure 15-16)**. Of note, last day's relative tumor growth values

revealed that combination treatment resulted in significantly smaller tumors compared to control and in case of H358 compared to tipifarnib treated tumors, also.

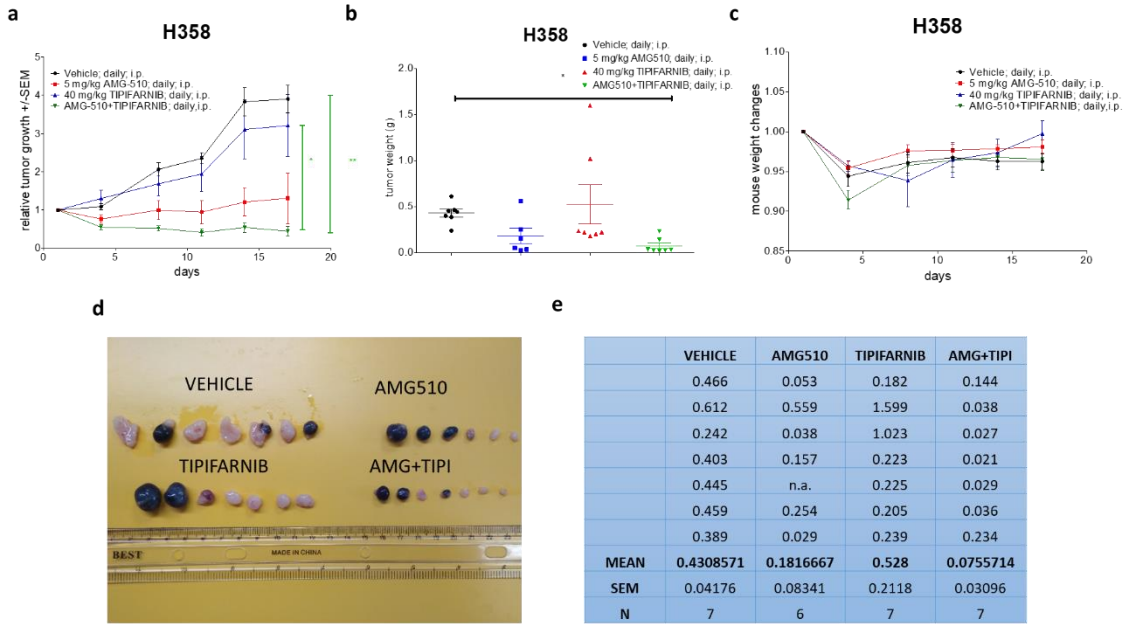

	VEHICLE	AMG510	TIPIFARNIB	AMG+TIPI
	0.466	0.053	0.182	0.144
	0.612	0.559	1.599	0.038
	0.242	0.038	1.023	0.027
	0.403	0.157	0.223	0.021
	0.445	n.a.	0.225	0.029
	0.459	0.254	0.205	0.036
	0.389	0.029	0.239	0.234
MEAN	**0.4308571**	**0.1816667**	**0.528**	**0.0755714**
SEM	0.04176	0.08341	0.2118	0.03096
N	7	6	7	7

Figure 15 *In vivo* tumor growth of H358 xenografts upon AMG510 (5 mg/kg i.p.) and/or tipifarnib (40 mg/kg i.p.) therapy. **a** Tumor volume was determined twice per week using caliper. Relative tumor volume growths are shown on the graph. Combinational treatment resulted significantly smaller tumor compared to control and tipifarnib treated tumors based on last day's relative growth values (tested with Kruskal-Wallis test followed by Dunn's Multiple Comparison Test; $p<0.05$). **b** and **e** Tumor weights (g) of H358 xenografts at day 18. Only combinational treatment resulted in significant effect compared to control (based on Kruskal-Wallis test followed by Dunn's Multiple Comparison Test; $p<0.05$). **d** Picture of the harvested tumors **c** Mouse weight loss during the treatment (day1=1).

Only combinational treatment was able to block tumor growth in H358 xenografts compared to control based on tumor weight (**Figure 15B**). To assess the toxicity associated with the drug treatment, body weights were monitored throughout the course of the study. Body weight losses were not significantly different between treatment groups (**Figure 15C**)

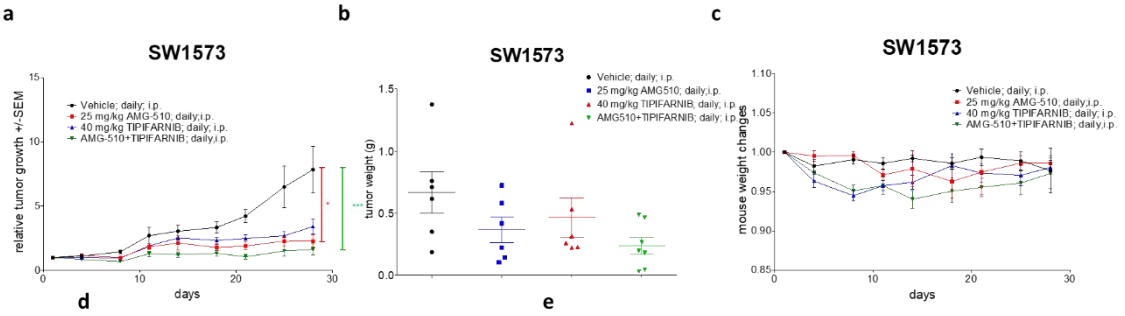

d

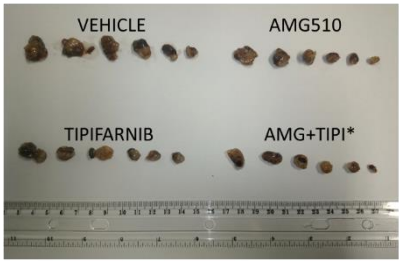

e

	VEHICLE	AMG510	TIPIFARNIB	AMG+TIPI
	0.351	0.1025	0.5323	0.0318
	0.76	n.a.	0.2277	0.4871
	n.a	0.7238	0.3143	0.4632
	0.6163	0.2227	n.a	0.266
	1.377	0.144	0.2239	0.1962
	0.7105	0.5804	0.2604	0.1802
	0.1855	0.4184	1.2243	0.0455
MEAN	**0.666717**	**0.3653**	**0.463817**	**0.238571**
SEM	0.1682	0.1026	0.1592	0.0687
N	6	6	6	7

Figure 16 *In vivo* tumor growth of SW1573 xenografts upon AMG510 (25 mg/kg i.p.) and/or tipifarnib (40 mg/kg i.p.) therapy. **a** Tumor volume was determined twice per week using caliper. Relative tumor volume growths are shown on the graph. AMG510 monotherapy and combinational therapy resulted in significantly smaller tumor compared to control based on last day's relative growth values (tested with Kruskal-Wallis test followed by Dunn's Multiple Comparison Test; $p<0.05$) **b** and **e** Tumor weights (g) of SW1573 xenografts at day 28. No statistically significant differences could be established (tested with one-way ANOVA) **d** Picture of the harvested tumors (*the smallest tumor of the AMG510+tipifarnib group was not included by accident). **c** Mouse weight loss during the treatment (day1=1)

4.11 MAPK and PI3K/AKT signaling pathway analysis

We have analyzed the effect of AMG510 and tipifarnib or combined treatment on ERK1/2, AKT and S6 activation and expression of RHEB and KRAS4B via immunoblot assay (**Figure 17**). Three independent measurement were performed, and bands were analyzed by densitometry (**Figure 18**).

We observed pronounced changes in the activation status of both signaling pathways, however, these changes varied among cell lines. The most robust effect on MAPK and PI3K/AKT pathway inhibition was observed on H358, where p-ERK, p-AKT and p-S6 levels significantly decreased upon AMG510 and combination treatment. AMG510 or combination treatment also decreased activation of ERK in SW1573 and PF139 cells. Interestingly, in H1792 cells tipifarnib and combination treatment robustly reduced p-S6 level, but elevated the level of p-ERK (**Figure 17-18**).

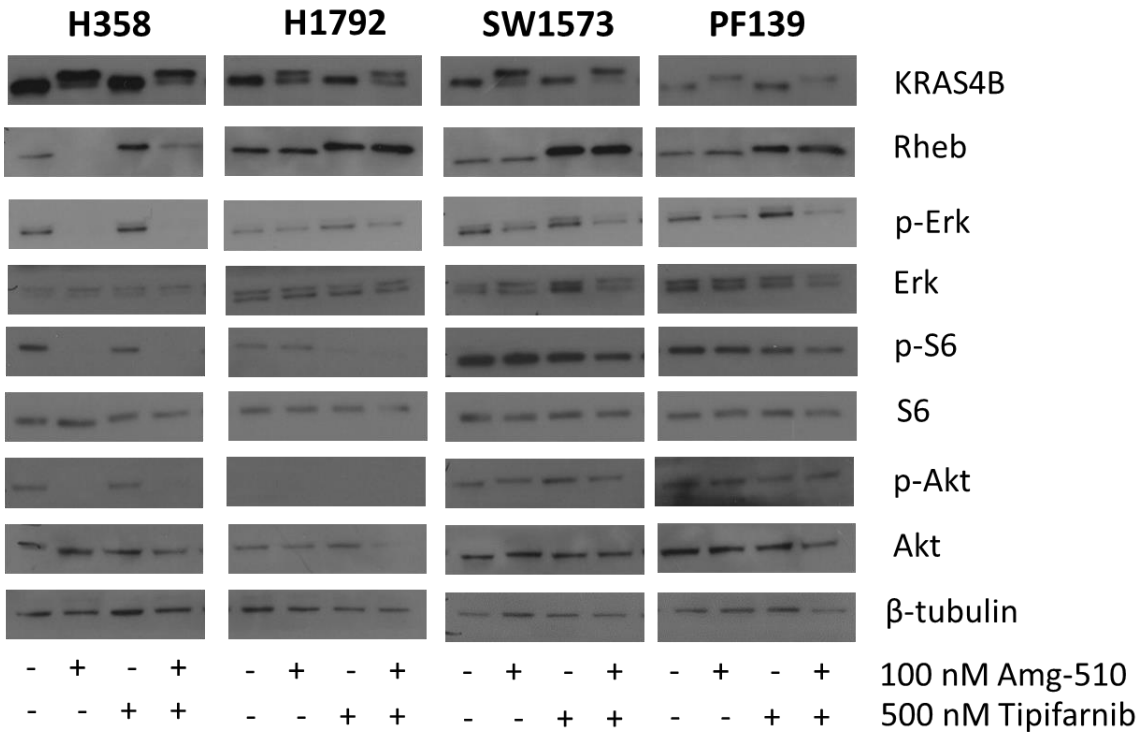

Figure 17 Representative blots of 48-hour treatment with 100 nM AMG510, 500 nM tipifarnib or combination. Note the upward shift of RHEB upon farnesylation inhibition and of KRAS upon AMG510 treatment.

Activation level of S6 decreased upon all treatment in H1792 and H358 cell lines. However, while neither monotherapy could reduce p-S6 activation at the two AMG510 resistant cell line (PF139, SW1573), it was slightly reduced upon combination treatment. Since FTIs inhibit prenylation of certain small G-proteins, we tested the expression of RHEB that is a member of the PI3K pathway. We observed an electrophoretic mobility shift of RHEB in each cell lines upon treatment with tipifarnib and combination, which represents the unprenylated (upper line) and prenylated (lower line) protein. These results demonstrated inhibition of farnesylation by tipifarnib. Treatments did not change KRAS4B expression remarkably neither of the cells. Interestingly, electrophoretic mobility shift was observed upon AMG510 treatment.

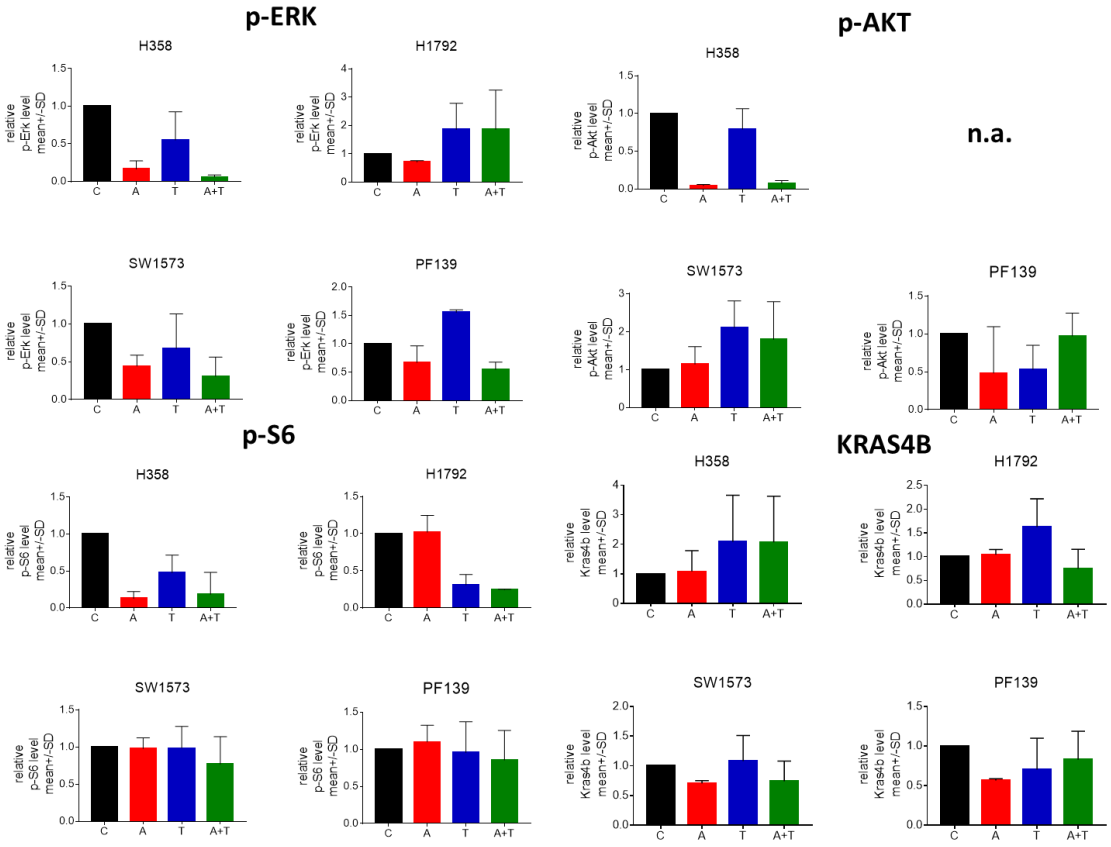

Figure 18 Densitometric analysis of immunoblot experiments shown in Figure 17. Results are from three independent experiments (mean, SEM). All data was normalized to total protein (based on Ponceau staining, not shown) and to control protein level. Cell signaling shows various changes upon treatment. No signal could be detected investigating p-AKT in H1792. Combinational treatment showed higher inhibitory effects on pS6 in all cell lines and p-ERK in all lines except for H1792. KRAS level was elevated as a result of tipifarnib treatment in H358 and H1792 cell lines.

4.12 Cell cycle distribution and apoptosis induction

The distribution of the cells in the cell cycle phases was determined after mono and combinational treatment based on DNA content (**Figure 19**). The ratio of cells in the G0/G1 phase was increased by the AMG510 and combination treatment in H358 cell line on 48 hours treatment. In the other three cell lines (H1792, SW1573, PF139) cell cycle phases did not change remarkably even after 96 hours long treatment. Tipifarnib and combinational treatment slightly increased G2/M phase cells in all cell lines. In line with this finding, we observed delayed cytokinesis in SW1573 time-lapse videomicroscopy upon tipifarnib treatment (data not shown).

Regarding the subG1 phase, the highest increase was observed also in H358 and H1792 upon AMG510 and combination treatment, while tipifarnib and combination slightly elevated level of subG1 cells in SW1573 (**Figure 19**). Furthermore, we also investigated the apoptosis induction via Western blot by cleaved-PARP/PARP protein detection (**Figure 20**).

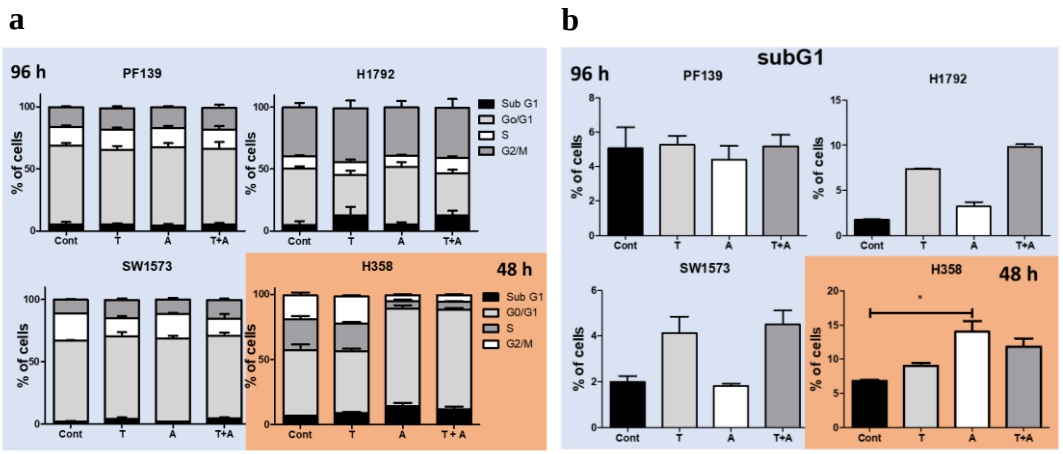

Figure 19 Cell cycle analysis of LUAD cells with 100 nM AMG510 (A), 500 nM Tipifarnib (T) or combination (A+T). **A** Changes in cell cycle distribution upon treatment. Most dramatic changes could be observed in H358 upon AMG510 treatment. B Apoptosis induction based on elevated subG1-phase cells. Tipifarnib and combinational treatment successfully increased subG1-phase in all cells except for PF139. Statistical analysis were carried out using non-parametric Kruskal-Wallis followed by post hoc Dunn's multiple comparison test.

We found that AMG510 and combination treatment was able to induce PARP cleavage in H358 and H1792 cells. We could observe only slight apoptosis induction based on PARP cleavage upon tipifarnib and combination treatment on SW1573 cells. Proliferating cell marker - PCNA protein - expression was also determined, and we found that combination treatment decreased PCNA expression in each cell lines except for SW1573 (**Figure 20 a-b**). We have performed time-lapse videomicroscopic analysis of *in vitro* 2D mitotic activity of SW1573 tumor cells, which can be characterized with relatively high proliferative capacity (data not shown).

We found in 72 hour-long experiments that following 24-hour exposure to drugs, combinational treatment drastically decreased the number of mitoses compared to both control and mono-treatments (**Figure 20C**).

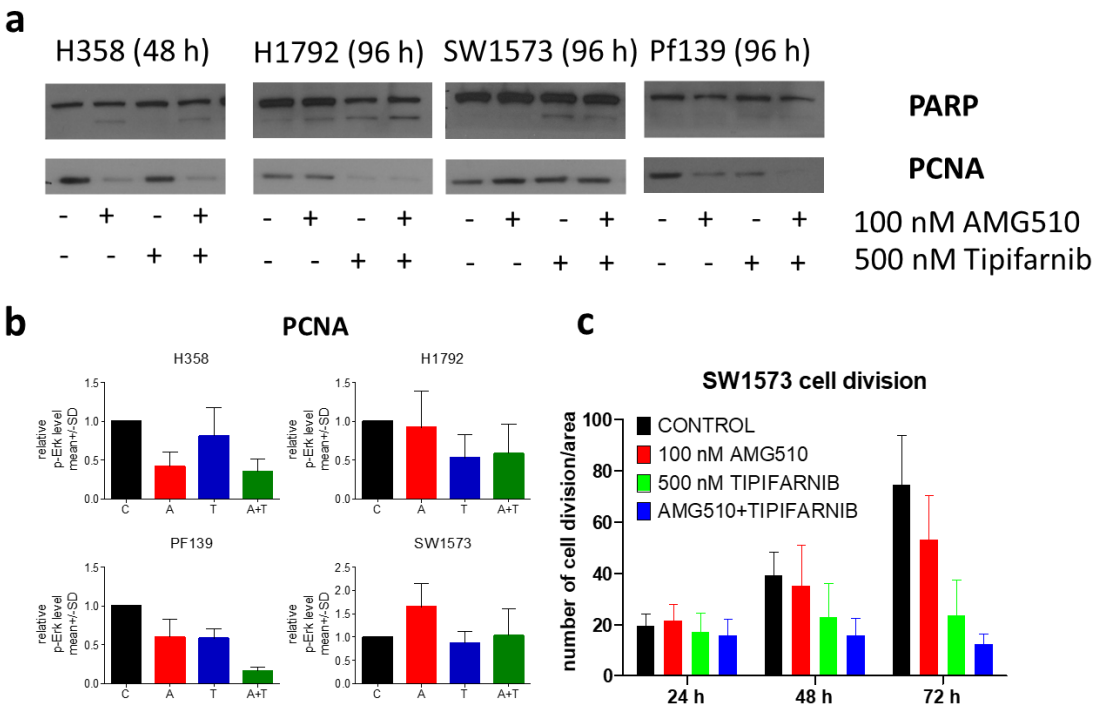

Figure 20 Apoptosis induction and mitotic activity of LUAD cells upon 100 nM AMG510 and/or 500 nM tipifarnib treatment. **A** AMG510 and combination treatment was able to induce apoptosis based on PARP cleavage in H358, H1792 and SW1573 cells. **B** PCNA protein expression decreased upon combination treatment in H358, PF139 but not in SW1573. **C** Effect of mono and combinational treatment with AMG510 (100 nM) and tipifarnib (500 nM) on mitotic capacity of SW1573 cells. Data derives from manual counting of mitoses of cells in three representative square from each field of view throughout treatment. One field of view was used in each well, and three well per treatment group was used in each experiment. Data are from three independent experiments.

5. Discussion

Aim of this thesis was to re-investigate the concept of prenylation inhibition as potential anticancer therapy with special emphasis on its association with *KRAS* mutation in colorectal and lung adenocarcinoma. Specifically, we compared a lipophilic, recently developed bisphosphonate with no affinity to bone material to clinically applied ZA using various preclinical models. We also investigated *in vitro* effects of bisphosphonate therapy on presence or absence of oncogenic *KRAS* mutation using isogeneic knockout cell models. Furthermore, using a publicly available database, we examined *KRAS* mutation dependent effects of three clinically applied classes of prenylation inhibitors on a large scale: statins, bisphosphonates and farnesyl-transferase inhibitors. Finally, we also investigated the combination of FTis with novel KRAS G12C mutation specific inhibitors.

5.1 Investigation and comparison of anti-tumor effects of the recently developed lipophilic bisphosphonate BPH1222 with the clinically approved zoledronate

Zoledronate (ZA) is a conventional, hydrophilic bisphosphonate that is currently used for treatment of osteoporosis and bone metastases. Recently, its lipophilic derivative, BPH1222 was developed [91].

Direct antitumor effects of ZA have been demonstrated in several preclinical study. In early works ZA turned out to possess the highest antitumor effect on breast cancer cells in comparison with other bisphosphonates such as aminobisphoshonate pamidronate and EB 1053, or a non-nitrogenous bisphosphonate, clodronate [79]. Furthermore, ZA also induced apoptosis and blocked proliferation using pancreatic cells *in vitro*. [82]. ZA exerted anti-proliferative and pro-apoptotic effects *in vitro* and also successfully blocked tumor growth of colorectal cells *in vivo* [113, 114].

However, bisphosphonates (including ZA) are well-known to possess high affinity to bone material that excludes their applicability for non-bone related events[115]. In an effort to expand usability of bisphosphonate therapy, lipophilic bisphosphonates with hydrophobic side-chains have been established [116]. Hydrophobicity of these drugs effectively prevented their accumulation in bone with significantly longer plasma half-

life compared to conventional bisphosphonates. Of note, they were found to be potent anticancer agents *in vitro* as well as *in vivo* using lung cancer models. [91].

We also performed two-dimensional *in vitro* experiments with ZA and BPH1222 using colorectal cancer cell cultures. Dose-dependent inhibitory effect could be observed upon treatment with both drugs. Furthermore, distinct differences could be observed in regard to sensitivity to ZA and BPH1222, though these differences did not show any association with major oncogenic mutations of cells. Neither drug was exclusively superior to the other in any mutational groups based on *BRAF* and *KRAS* oncogenic alterations.

In a study investigating melanoma cells, 12-hour exposure to 100 μM ZA drastically increased number of apoptotic cells [84]. Another study using human breast cancer cell lines found that S-phase arrest and twofold increase in the number of apoptotic cells could be observed upon 24-hour treatment with 100 μM ZA [78]. Also, in colorectal cancer cell line HCT116 25 μM ZA treatment induced apoptosis marked by the presence of cleaved PARP [114] and also in other study demonstrated by flow cytometry analysis [113]. Also, induction of apoptosis was confirmed by TUNEL assay in colorectal cancer xenograft models following exposure to ZA [117]

We used significantly smaller concentration of bisphosphonate (10 μM) than used in the literature to get more physiologically relevant results and still observed a moderate but consequent increase in subG1- and/or S-phase. Efficacy of BPH1222 on inducing increased subG1-phase and S-phase block was more intense in comparison to ZA, although it was not statistically significant.

Based on distinct polarity of ZA and BPH1222, we examined their behavior and efficacy in 3D environment using multicellular tumor spheroid model. The spheroid model is considered to be more clinically relevant than conventional monolayer cultures as it mimics several aspects of *in vivo* conditions including cell-cell and cell-ECM interactions, distinct distribution and diffusion of drugs, oxygen and nutrients [118]. Of note, probably due to its lipophilic nature, BPH1222 inhibited stronger the spheroid growth compared to ZA in all cell lines. Interestingly, this result was independent not only from their mutational status but even from the results of clonogenic assays in monolayer experiments. In line with our 3D spheroid results, lipophilic bisphosphonates were demonstrated to be more potent in *in vivo KRAS*-mutant lung cancer models [91]. Our study also confirmed this finding as HCT116 xenografts carrying KRAS G13D

mutations was shown to be more sensitive to BPH1222 treatment in comparison with ZA. Inhibition of tumor growth by BPH1222 was statistically significant compared to control xenografts.

Both bisphosphonates failed to block tumor growth in *BRAF* V600E mutant SW1417 colorectal cancer xenograft model. Notably, though dose-dependent effects with both drugs were observed in SW1417 cells in vitro in 2D and 3D settings, this cell line was the only one where activation of S6 did not decrease upon treatment. Level of phosphorylated S6 has been shown to be an important marker of drug response [119]. In addition, 3D spheroid growth rate of SW1417 was found to be the highest among the cell lines investigated and 3D efficacy of both bisphosphonate was the lowest against this cell line among the four cell lines capable of spheroid formation. Colorectal tumors harboring *BRAF* V600E mutation have a poor prognosis, even when treated with vemurafenib, a mutation specific inhibitor, that failed to show clinical activity likely due to feedback reactivation of EGFR pathway [120].

Nevertheless, 3D spheroid data and *in vivo* experiment with *KRAS* G13D mutant HCT116 xenograft model unequivocally support higher potency of lipophilic BPH1222 in comparison to the currently most effective clinically applied ZA. Along with the fact that lipophilic bisphosphonates show no bone accumulation [91], our data strongly suggest clinical examination of this approach even in non-bone related application.

5.2 Investigation of effects of bisphosphonates on mutant K-RAS

We have previously showed that *PTEN* wild-type and *BRAF*-mutant melanoma cells were more resistant to ZA in comparison to *BRAF*-mutant and *PTEN* null or *NRAS*-mutant cells that showed profoundly lower proliferation and increase in apoptosis upon ZA exposure *in vitro* [85]. Concerning other molecular aberrations in the RTK signaling pathway, wild-type and mutant HER expressing cells were sensitive to ZA treatment in breast and lung cancer cells, while cells with low expression of HER were found to be resistant to it [80]. Furthermore, lipophilic bisphosphonate BPH1222 showed synergistic effects on KRAS-mutant lung cancer *in vitro* and *in vivo* models in combination with rapamycin [91].

Above mentioned scientific data show that inhibition of prenylation has pleiotropic – and not fully understood – effects on RTK signaling. Thus, we examined effects of ZA and BPH1222 exposure on RAS-related signaling. Interestingly, we found that prenylation

inhibition had strong effects on the activation of ERK and S6 of which phosphorylation level is commonly used for examining activation status of the two major signaling cascade regulated by RAS: RAF/MEK/ERK and PI3K/AKT, respectively.

Prenylation inhibitors strongly decreased level of p-S6 in all cell lines, except for SW1417. S6 is an important downstream component of the PI3K/mTOR cascade and is considered to integrate input signals from various signaling pathways that are essential for cell growth and survival. In line with this, reduced activation of S6 has been shown to be a sensitive marker for efficacy of drug treatment [119]. Our study confirms this observation as we found that SW1417 xenografts did not respond to treatment with ZA or BPH1222. Notably, treatment with bisphosphonates was not able to reduce level of p-S6 only in this particular cell line among our cell panel examined.

Interestingly, ZA and BPH1222 induced profound activation of ERK in all three cell lines carrying *KRAS* mutation as well as in *BRAF* V600E mutant SW1417, while in *KRAS* and *BRAF* wild type CACO2 and HCA7, and also in *BRAF* V600E mutant WIDR, no change could be observed on ERK activation. In order to examine whether changes in RAS signalization has any connections with presence of oncogenic KRAS protein, we repeated some of our experiments using two distinct isogeneic cellular model system on mutant KRAS. These models consist of isogeneic cell pairs with parental cell lines (DLD1 and HCT116) with heterozygous *KRAS* G13D mutations and their knockout derivatives (DKO4 and HKh-2, respectively) that has their KRAS G13D allele disrupted by homologous recombination. We observed significant differences in sensitivity only to BPH1222 treatment between parental cells and knockout derivatives. In addition, while bisphosphonate treatment elevated level of phosphorylated ERK in the parental cell lines (*KRAS* G13D/WT), it had only small or no effect in the knockout clones (-/WT). Of note, response to bisphosphonate regarding ERK activation resembled to what was observed in *KRAS* wild-type CACO2, HCA7 and WIDR cell lines.

We also found that DKO-4 (-/WT) knockout derivative of DLD1(G13D/WT), became more prone to BPH1222 exposure. In contrast, HKh-2 (-/WT), knockout clone of HCT116 (G13D/WT) apparently became less sensitive to BPH1222 treatment. Furthermore, both bisphosphonate drug induced significant apoptosis marked by the appearance of cleaved PARP in HCT116 (G13D/WT; TP53 WT). However, this response was almost completely abolished upon disruption of *KRAS* G13D allele in HKh-2 (-/WT;

TP53 WT), knockout derivative of HCT116. This result suggests that the ability of bisphosphonate drugs to induce apoptosis in this particular model was dependent on the presence of the oncogenic *KRAS* G13D allele. This is also true to other alterations in response to bisphosphonate treatment: changes in sensitivity or cell signaling. In summary, our results suggest that inhibition of prenylation by bisphosphonates interferes with oncogenic KRAS protein, even though this interaction is currently not fully understood and seems to be varying among cell lines.

5.3 Comparison of anticancer effects of different classes of prenylation inhibitors on different types of tumors in regard to their KRAS mutational status

On the way towards understanding prenylation inhibition and *KRAS*, we have to keep in mind that the tissue of origin may have strong influence on the biology of cells carrying mutant *KRAS* including their response to drug exposure [121]. For instance, it has been demonstrated that site of metastasis affect prognostic value of *KRAS*, underlining importance of context-dependent behavior and features of oncogenic *KRAS* [122-124]. Furthermore, distribution of specific mutations (e.g. abundance of *KRAS* G12C mutations in lung adenocarcinoma, or *KRAS* G13D in colorectal cancers) may also have an impact on tissue-dependent differences. For example, distinct intrinsic GTPase activity could be measured between KRAS G12C, G12V, G13D or Q61L mutations as well as differential sensitivity to GEF mediated activation or inactivation by GAP proteins [125, 126].

Accordingly, our results based on publicly available repurposing primary screen showed that efficacy of statins, bisphosphonates and farnesyl-transferase inhibitors varied between lung and colorectal cancer cell lines. Although statistically significant differences could only be seen comparing *KRAS* mutant LUAD cell lines to those with *RAS* wild type, opposite trends could be observed in response to drugs between lung and colorectal adenocarcinoma cells. More specifically, colorectal cells carrying *KRAS* mutation were more resistant to N-bisphosphonates ($p=0.12$) and farnesyl-transferase inhibitors ($p=0.17$) compared to *RAS* wild cells. In contrast, *KRAS* mutant LUAD cells were more responsive to treatment with N-bisphosphonates and to FTis ($p=0.136$ and $p=0.007$, respectively) than wild type cells.

Although not statistically significant, these results point out to potential tissue-specific differences in response to inhibition of prenylation in cells harboring *KRAS* mutation.

Furthermore, this analysis raises new questions, most importantly why farnesyl-transferase inhibitors exerted higher inhibitory potential on LUAD cells carrying *KRAS* mutations. Notably, alternative geranylgeranylation of KRAS has been demonstrated as a resistance mechanism in cells treated with FTis.

Distinct isoform expression patterns may also have an impact on the response to different classes of prenylation inhibitors. Interestingly, it was demonstrated that farnesyl-transferase enzymes have markedly the highest affinity to KRAS4B isoform, followed by KRAS4A [127]. It has been increasingly appreciated that KRAS4A isoform is also commonly expressed in various types of cancers that may have profound impact on signaling and regulation of KRAS [48]. Additionally, it was postulated that differential expression of distinct isoforms of *RAP1GDS1* gene leads to altered regulation of prenylation of small GTPases, including KRAS. Tumor progression in breast cancer and LUAD has been linked with elevated transcription of RAP1GDS1 [128-130]. Thus, differential expression of RAP1GDS1 may influence sensitivity of distinct tumor types towards prenylation inhibition.

As prenylation is an irreversible posttranslational modification, blockade of prenylation can only impact newly translated KRAS proteins. However, little or no data available concerning degradation and turnover rate of KRAS protein, although several proteins were proposed to be involved in regulation of KRAS degradation, like β-TRCP1 [131] NEDD41 [132] or Lztr1-cul3 [133]. It has also been shown that WNT/β-CATENIN signaling also regulates RAS stability through β –CATENIN that stabilizes RAS through binding to it. [134]. Alterations of WNT pathway are frequently found in colorectal cancer that result in stabilization of β –CATENIN [135] and may affect response to inhibition of prenylation leading to a more resistant phenotype.

5.4 The combination of clinically approved drug classes with the novel KRAS G12C inhibitor Sotorasib (AMG510) on KRAS G12C mutant lung adenocarcinoma cell lines

KRAS is one of the most commonly mutated oncogenes and raises huge challenges for oncologists and cancer researchers [52]. For decades, mutant KRAS was considered “undruggable” due to several distinct features of this small, compact protein. Moreover,

mutation of KRAS is also a negative predictive factor against anti-EGFR therapies [125, 136]. Recently new mutant allele-specific inhibitors were developed against KRAS G12C oncoprotein, some of them already entering the clinics [53]. While this approach holds great promises, especially in lung adenocarcinoma tumors, where *KRAS* G12C mutation represents ~40% of all *KRAS* mutations, resistance against these inhibitors also emerged. Partial response was only observed in 32.2% of LUAD and 7.1% of colon cancer patients. Majority of patients (56.9% in LUAD, 66,7% in colon cancer) had stable disease, while tumors of 8,5% of LUAD and 23,8% of colorectal cancer patients progressed [137]. Thus, combination studies are urgently needed for breaking down resistance and enhance efficacy of this promising approach. Clinical trials with various combinations are ongoing testing immunotherapy, SHP2, SOS1 or EGFR inhibitors, among others [54].

Our findings that FTis showed higher antitumor activity in KRAS mutant LUAD cell lines compared to those with wild type RAS proteins points to a potential new combinational approach. Farnesyl-transferase inhibitors (e.g. tipifarnib and lonafarnib) initially was developed against tumors carrying RAS mutation and were the center of attention at the millennium. Through blocking farnesylation of RAS proteins, FTis were expected to inhibit RAS signaling by inducing mislocalization of these oncoproteins. However, clinical trials showed no clinical benefit upon FTi treatment [138]. Further studies concluded that failure of these drugs was due to alternative geranylgeranylation of KRAS and NRAS protein that ensured their proper localization even in the presence of FTis [43]. Notably, HRAS is known only be able to be farnesylated, and clinical trials of tipifarnib against *HRAS* mutant tumors are ongoing [31]. Besides, lonafarnib has just been approved for treatment of progeria showing along with previous clinical trials that FTis are safe and applicable [97]. In conclusion, although they lack clinical efficacy against *KRAS* mutant tumors as monotherapy, these drugs have well studied clinical behavior, including toxicity and therapeutic window.

Our previous results show that *KRAS* mutant LUAD cell lines are significantly more sensitive to FTis. Further analyzing these results we showed that increased sensitivity of *KRAS* mutant LUAD cell lines compared to wild *RAS* LUADS was due mainly to presence of several *KRAS* G12C cell lines among them (data not shown).

We also tested this phenomenon on our panel of G12C *KRAS* mutant LUAD cell lines. We combined *KRAS* G12C inhibitors with FTIs and found that addition of this drug

resulted in robust and reproducible synergy. We used four *KRAS* G12C mutant lung adenocarcinoma with distinct sensitivity against KRAS G12C treatment. Besides conventional 2D tests, we also investigated more relevant 3D tumor spheroids of the LUAD cell lines treated with AMG510 and tipifarnib. Interestingly, SW1573, highly resistant against AMG510 in 2D become much more sensitive cultured as tumor spheroids, in accordance with published literature showing that *KRAS* dependence are more pronounced in 3D conditions. Synergy was found to be the strongest on the two AMG510 resistant cell lines, PF139 and SW1573.

Interestingly, combining other drugs resulted in similar results, for example AMG510 combined with lonafarnib (another farnesyl-transferase inhibitor) or ARS-1620 (an earlier KRAS G12C inhibitor) with tipifarnib. However, when we tested other prenylation inhibitors like statins, N-bisphosphonates or even geranylgeranyl-transferase inhibitors in combination with KRAS G12C inhibitors, we found no synergistic effects on the tumor cell lines (data not shown). This result indicates that the mechanism behind the synergy is based solely on inhibition of farnesylation combined with KRAS G12C targeting.

Furthermore, we wanted to investigate potential clinical applicability of FTis using *in vivo* preclinical models. We included one AMG510 sensitive (H358) and one resistant (SW1573) LUAD cell lines for subcutaneous xenograft experiments. We found that monotherapy with AMG510 effectively blocked tumor growth in both experiments. This finding outlines the importance of our spheroid experiments with SW1573, which predicted that in 3D conditions, higher *KRAS* dependence could be expected. Interestingly, tipifarnib alone also effectively inhibited tumor growth of SW1573. In both experiment combinational treatment had the highest antitumoral activity as demonstrated by both volume measuring along the experiment and the weight of tumors (FIG). Of note, no treatment related toxicity was observed during the experiments. These results confirm our 2D and 3D *in vitro* experiments and show that combination of FTis along with mutant KRAS G12C specific inhibitors is an effective and feasible option for treatment of lung adenocarcinoma tumors harboring KRAS G12C mutation.

5.5 The mechanism for synergistic effects of combinational therapy using FTis and KRAS G12C inhibitors

Though inhibition of farnesylation is known to have pleiotropic effects that are hard to investigate [31], we performed some mechanistic studies in order to find the underlying mechanism behind these robust synergistic effects. First, we performed immunoblot analysis investigating KRAS related signaling cascades. Interestingly, we found profound changes in RAF/MEK/ERK and PI3K/AKT/MTOR pathways upon single agent and combinational treatments, though the responses varied among cell lines. While AMG510 was able to inhibit activation of ERK in each analyzed cell lines, it could only decrease level of p-S6 on the two most AMG510 sensitive cell lines H358 and H1792. Interestingly, phosphorylation status of AKT did not mirrored changes in level of p-S6. In contrast, in the AMG510 resistant cell lines PF139 and SW1573 activation of S6 could only be decreased by combinational treatment. Regarding AKT activation, we could not detect p-AKT in H1792 at all, and the other three cell lines also showed mixed results. While no consistent changes could be observed in the cell lines analyzed, these results suggest that interference with RAS signaling pathways may partly mediate synergistic effects of the investigated combination.

We also investigated changes of KRAS4B and RHEB protein levels. We found that KRAS4B shows a clear upward shift upon AMG510 treatment, a finding that can be observed in other publications using KRAS G12C inhibitors [112, 139]. However, this phenomenon still lacks any scientific explanation. Tipifarnib and combinational treatment elevated KRAS level only in H358 treatment, thus changes in KRAS level are probably not responsible for synergistic effects. We validated successful inhibition of farnesylation investigating RHEB protein, a small farnesylated GTPase that is part of the PI3K/AKT/MTOR pathway. We observed small, but clearly visible upward shift upon tipifarnib and combinational treatment showing the accumulation of unfarnesylated RHEB. Of note, this observed effect of FTis is in line with available scientific literature [140]. One of thepossible explanations is that without farnesylation, the last three amino acids would not be removed, resulting in a slightly heavier protein that localize upward of the normally farnesylated protein band.

Indeed, confirmed by the successful inhibition of RHEB farnesylation, we suggest that inhibition of prenylation of several other small GTPases may be responsible for the strong synergy observed. Small GTPases, like RHEB, RHO, RAC, and RAP1A play important part in many cellular processes and signaling pathways controlling proliferation,

migration, changes in cytoskeleton, among others [93-95, 141]. Many of these processes were also connected to RAS signaling, therefore their inhibition along with blocking mutant KRAS activity may as well be responsible for synergistic anti-tumor activity.

Furthermore, we also analyzed how treatment affects cell cycle and apoptosis. Interestingly, all cell lines analyzed showed only minor alterations on cell cycle distribution, except for H358 where even after 48-hours treatment ratio of G0/G1 phase cells was found to be drastically elevated suggesting block of G1-S entry. Interestingly, proliferation marker PCNA was drastically inhibited by combinational treatment in H358, H1792 and PF139. However, no changes could be observed in SW1573.

Strong apoptosis induction was observed based on accumulation of subG1 cells and cleaved PARP in H358 and H1792 upon AMG510 and combination treatment. Tipifarnib and combinational treatment slightly elevated both level of subG1 cells and cleaved PARP in SW1573 cells, while no apoptosis induction could be observed in PF139 cells. Interestingly, none of the end-point measurement of PCNA, PARP and cell cycle in SW1573 could provide explanation for the robust synergy between KRAS G12C inhibitor and FTis on this cell line. However, 72-hours-long time-lapse videomicroscopy revealed robust decrease in proliferation in response to tipifarnib, and even more profoundly, to combination treatment. Of note, only a small extent of apoptotic cells could be observed in the videos analyzed (data not shown). Thus, most probably inhibition of proliferation could be accounted for the observed synergistic effects, demonstrated by immunoblot analysis of PCNA and time-lapse videomicroscopy.

In conclusion of our mechanistic studies, distinct and various effects were observed upon single agent and combinational treatments in the cell lines analyzed. Given the multitude of potential resistance mechanisms, farnesyl-transferase inhibitors are favorable candidates for combination with KRAS G12C inhibitors, as their pleiotropic effects may effectively shut down different escape routes of *KRAS* mutant tumors.

6. Conclusions

Aim of this thesis was to re-investigate applicability of clinically approved inhibitors of prenylation as anticancer agent with special emphasis on their association with oncogenic KRAS. We present our findings below with our objectives from the Aims section.

Comparison of anti-tumor effects of a recently established lipophilic bisphosphonate with the clinically approved zoledronate.

Our data using different colorectal cancer models established strong basis for further investigation and potential applicability of lipophilic BPH1222 that exerted significantly higher antitumor activity in comparison with zoledronate, which is a clinically approved and widely used N-bisphosphonate. Importantly, lipophilic bisphosphonates could be used in tumors not affecting bones.

Investigation of effects of bisphosphonates on mutant KRAS and comparison of anticancer effects of different classes of prenylation inhibitors on different types of tumors in regard to their KRAS mutational status.

Our data on *KRAS* knockout colorectal cancer cell models suggest mutant *KRAS* dependent effects of N-bisphosphonate treatment. Furthermore, large scale *in silico* analysis utilizing different classes of prenylation inhibitors (statins, N-bisphosphonates and farnesyl-transferase inhibitors) showed that *KRAS* mutational status and tissue of origin markedly affect sensitivity towards these drugs. Of note, *KRAS* mutant lung adenocarcinoma cell lines were significantly more sensitive to FTi treatment than wild type cells.

Overall, our studies suggest that inhibition of prenylation exerts anticancer effects on cells harboring *KRAS* mutations and interfere with biological functions of *KRAS* as well as with RAS-related signaling. However, these effects are probably indirect and do not impact KRAS protein directly.

Examine potential combinational strategy using clinically approved drug classes with the novel KRAS G12C inhibitor Sotorasib (AMG510) on KRAS G12C mutant lung adenocarcinoma cell lines.

Finally, we investigated combination therapy of novel KRAS G12C inhibitor AMG510 (Sotorasib) with the farnesyl-transferase inhibitor tipifarnib. Strikingly, robust synergistic effects emerged between these drug classes in various *in vitro* and also *in vivo* settings. Notably, farnesyl-transferase inhibitors (like tipifarnib and lonafarnib) are also tested in the clinics and have favorable, well-known safety profile. The synergistic anti-tumor effects of FTis in combination with novel KRAS G12C allele specific inhibitors therefore have high clinical relevance.

7. Summary

KRAS is one of the most frequently mutated oncogenes; ~30% of colorectal cancer and up to 16% of lung adenocarcinoma cases carry *KRAS* mutations. However, except for the *KRAS* G12C mutation no targeted therapy is available for the treatment of *KRAS* mutant tumors. Furthermore, earlier failure of the farnesyl-transferase inhibitors heavily impaired efforts for indirect targeting of this oncogene. Aim of this thesis was to investigate the impact of different classes of clinically approved prenylation inhibitors on *KRAS* mutant colorectal and lung adenocarcinoma.

In contrast to FTis, N-bisphosphonates can block both farnesylation and alternative geranylgeranylation of the RAS proteins. However, due to their high affinity to bone minerals, their application is limited to bone related events. In order to overcome this obstacle, lipophilic bisphosphonates were developed. Using conventional monolayers (2D), multicellular spheroids (3D) and xenograft models (*in vivo*) of colorectal cancer, we demonstrated that lipophilic BPH1222 was more efficient than the clinically approved zoledronic acid in 3D and in vivo settings. Furthermore, we also showed that treatment with BPH1222 results in distinct changes in signaling and drug sensitivity that depends on the presence of the *KRAS G13D* mutation.

We also analyzed the *KRAS* mutation dependent sensitivity towards statins, N-bisphosphonates and farnesyl-transferase inhibitors using publicly available data of PRISM Repurposing Primary Screen. Interestingly, we found that farnesyl-transferase inhibitors exerted significantly higher antitumor activity on *KRAS*-mutant LUAD cells compared to those with wild type RAS. As 40% of *KRAS* mutant lung adenocarcinoma cases harbor *KRAS* G12C mutation, we further investigated whether FTis could enhance anticancer effects of recently developed KRAS G12C specific inhibitors. Surprisingly, we found that combination of FTis with KRAS G12C inhibitors resulted in robust synergistic effects on all cell lines investigated in 2D, 3D and *in vivo* settings. Combinational treatment resulted in various profound changes in KRAS related signalization, inhibition of proliferation and induction of apoptosis.

In summary, our results show that inhibition of prenylation can be a useful tool for treatment of *KRAS* mutant colorectal or lung tumors. Furthermore, combination of farnesyl-transferase inhibitors with Sotorasib can be an efficient strategy for breaking down resistance against KRAS G12C specific inhibitors.

8. Összefoglalás

A *KRAS* gén egyike a leggyakrabban mutációt szenvedő protoonkogéneknek: a kolorektális tumorok ~30%-a, valamint a tüdő adenokarcinómák 16%-a hordoz *KRAS* mutációt. Ennek ellenére, jelenleg a *KRAS* G12C mutáns eseteken kívül nincs elérhető célzott terápia a *KRAS* mutációt hordozó tumorokra. Jelen doktori munka célja a klinikumban is elérhető különböző típusú preniláció gátló hatóanyagok hatásának vizsgálata *KRAS* mutáns kolorektális és tüdő adenokarcinóma preklinikai modelleken.

A farnezil-transzferáz inhibitorokkal (FTi) ellentétben az aminobiszfoszfonátok képesek mind a RAS farnezilációt, mind az alternatív geranilgeranilációt gátolni. Ugyanakkor perceken belül lerakódnak a csontok szervetlen állományába, így csonthoz köthető elváltozások (csontritkulás, csontáttét) terápiájában van szerepük. A közelmúltban kifejlesztett lipofil biszfoszfonátok nem mutatnak csontszelektivitást, így más területeken is felhasználatóak lehetnek. Kísérleteink alapján az újonnan kifejlesztett lipofil BPH1222 hatékonyabbnak bizonyult a klinikumban is használt zoledronsavhoz képest 3D környezetben és *in vivo* egyaránt kolorektális tumorsejtek preklinikai modelljein. Ezen felül kimutattuk, hogy a BPH1222 kezelésre mutatott érzékenység, valamint az általa okozott jelátviteli változások részben a *KRAS* G13D mutáns allél jelenlététől függenek.

A PRISM Repurposing Primary Screen nyilvánosan elérhető adatbázisa alapján megvizsgáltuk a sztatinok, aminobiszfoszfonátok és FTi-k *KRAS* mutáns státusz függő hatását. Érdekes módon a *KRAS* mutációt hordozó tüdő adenokarcinóma sejtvonalak fokozott érzékenységet mutattak az FTi kezelésre. A *KRAS* mutáns tüdő adenokarcinómák körülbelül 40%-át *KRAS* G12C mutációk alkotják, így szerettük volna megvizsgálni, hogy a farnezil-transzferáz inhibitorok képesek-e erősíteni az új KRAS G12C inhibitorok tumorellenes hatásait. Meglepő módon a kombináció rendkívül robosztus szinergizmust mutatva gátolta a *KRAS* G12C mutáns tüdő adenokarcinóma sejtvonalak növekedését 2D, 3D és *in vivo* körülmények között is. A kombinációs kezelés hatására a KRAS által szabályozott jelátvitel sejtvonalanként eltérő erőteljes változásokat mutatott, ezen felül apoptózist és az osztódási aktivitás gátlását eredményezte.

Eredményeink alapján a preniláció gátlása hatékony terápiás eszköz lehet *KRAS* mutációt hordozó kolorektális és tüdő tumorokra. Az FTi-k kombinációja KRAS G12C inhibitorokkal kiemelten hatékony terápiás eszköz lehet *KRAS* G12C mutációt hordozó tüdő adenokarcinómától szenvedő betegek kezelésére.

9. References

1. Prior, I.A., P.D. Lewis, and C. Mattos,(2012) *A comprehensive survey of Ras mutations in cancer.* Cancer Res. **72**(10): p. 2457-2467.
2. Prior, I.A., F.E. Hood, and J.L. Hartley,(2020) *The Frequency of Ras Mutations in Cancer.* Cancer Res. **80**(14): p. 2969-2974.
3. Chen, K., Y. Zhang, L. Qian, and P. Wang,(2021) *Emerging strategies to target RAS signaling in human cancer therapy.* J Hematol Oncol. **14**(1): p. 116.
4. Bos, J.L., H. Rehmann, and A. Wittinghofer,(2007) *GEFs and GAPs: critical elements in the control of small G proteins.* Cell. **129**(5): p. 865-877.
5. Gorfe, A.A., B.J. Grant, and J.A. McCammon,(2008) *Mapping the nucleotide and isoform-dependent structural and dynamical features of Ras proteins.* Structure. **16**(6): p. 885-896.
6. Stolze, B., S. Reinhart, L. Bulllinger, S. Frohling, and C. Scholl,(2015) *Comparative analysis of KRAS codon 12, 13, 18, 61, and 117 mutations using human MCF10A isogenic cell lines.* Sci Rep. **5**: p. 8535.
7. Waring, P., J. Tie, D. Maru, and C.S. Karapetis,(2016) *RAS Mutations as Predictive Biomarkers in Clinical Management of Metastatic Colorectal Cancer*. Clin Colorectal Cancer. **15**(2): p. 95-103.
8. Simanshu, D.K., D.V. Nissley, and F. McCormick,(2017) *RAS Proteins and Their Regulators in Human Disease.* Cell. **170**(1): p. 17-33.
9. Hunter, J.C., A. Manandhar, M.A. Carrasco, D. Gurbani, S. Gondi, and K.D. Westover,(2015) *Biochemical and Structural Analysis of Common Cancer-Associated KRAS Mutations.* Mol Cancer Res. **13**(9): p. 1325-1335.
10. Ahearn, I., M. Zhou, and M.R. Philips,(2018) *Posttranslational Modifications of RAS Proteins.* Cold Spring Harb Perspect Med. **8**(11).
11. Zhang, S.Y., B. Sperlich, F.Y. Li, S. Al-Ayoubi, H.X. Chen, Y.F. Zhao, Y.M. Li, K. Weise, R. Winter, and Y.X. Chen,(2017) *Phosphorylation Weakens but Does Not Inhibit Membrane Binding and Clustering of K-Ras4B.* ACS Chem Biol. **12**(6): p. 1703-1710.
12. Fivaz, M. and T. Meyer,(2005) *Reversible intracellular translocation of KRas but not HRas in hippocampal neurons regulated by Ca2+/calmodulin.* J Cell Biol. **170**(3): p. 429-441.

13. Zhou, Y., P. Prakash, A.A. Gorfe, and J.F. Hancock,(2018) *Ras and the Plasma Membrane: A Complicated Relationship.* Cold Spring Harb Perspect Med. **8**(10).
14. Gulyas, G., G. Radvanszki, R. Matuska, A. Balla, L. Hunyady, T. Balla, and P. Varnai,(2017) *Plasma membrane phosphatidylinositol 4-phosphate and 4,5-bisphosphate determine the distribution and function of K-Ras4B but not H-Ras proteins.* J Biol Chem. **292**(46): p. 18862-18877.
15. Pylayeva-Gupta, Y., E. Grabocka, and D. Bar-Sagi,(2011) *RAS oncogenes: weaving a tumorigenic web.* Nat Rev Cancer. **11**(11): p. 761-774.
16. Hanahan, D. and R.A. Weinberg,(2011) *Hallmarks of cancer: the next generation.* Cell. **144**(5): p. 646-674.
17. Drosten, M. and M. Barbacid,(2020) *Targeting the MAPK Pathway in KRAS-Driven Tumors.* Cancer Cell. **37**(4): p. 543-550.
18. De Luca, A., M.R. Maiello, A. D'Alessio, M. Pergameno, and N. Normanno,(2012) *The RAS/RAF/MEK/ERK and the PI3K/AKT signalling pathways: role in cancer pathogenesis and implications for therapeutic approaches.* Expert Opin Ther Targets. **16 Suppl 2**: p. S17-27.
19. Jafari, M., E. Ghadami, T. Dadkhah, and H. Akhavan-Niaki,(2019) *PI3k/AKT signaling pathway: Erythropoiesis and beyond.* J Cell Physiol. **234**(3): p. 2373-2385.
20. Alzahrani, A.S.,(2019) *PI3K/Akt/mTOR inhibitors in cancer: At the bench and bedside.* Semin Cancer Biol. **59**: p. 125-132.
21. Kimmelman, A.C.,(2015) *Metabolic Dependencies in RAS-Driven Cancers.* Clinical Cancer Research. **21**(8): p. 1828-1834.
22. Ying, H.Q., A.C. Kimmelman, C.A. Lyssiotis, S.J. Hua, G.C. Chu, E. Fletcher-Sananikone, J.W. Locasale, J. Son, H.L. Zhang, J.L. Coloff, H.Y. Yan, W. Wang, S.J. Chen, A. Viale, H.W. Zheng, J.H. Paik, C. Lim, A.R. Guimaraes, E.S. Martin, J. Chang, A.F. Hezel, S.R. Perry, J. Hu, B.Y. Gan, Y.H. Xiao, J.M. Asara, R. Weissleder, Y.A. Wang, L. Chin, L.C. Cantley, and R.A. DePinho,(2012) *Oncogenic Kras Maintains Pancreatic Tumors through Regulation of Anabolic Glucose Metabolism.* Cell. **149**(3): p. 656-670.

23. Zago, G., M. Biondini, J. Camonis, and M.C. Parrini,(2019) *A family affair: A Ral-exocyst-centered network links Ras, Rac, Rho signaling to control cell migration.* Small GTPases. **10**(5): p. 323-330.
24. Rosse, C., A. Hatzoglou, M.C. Parrini, M.A. White, P. Chavrier, and J. Camonis,(2006) *RalB mobilizes the exocyst to drive cell migration.* Mol Cell Biol. **26**(2): p. 727-734.
25. Oxford, G., C.R. Owens, B.J. Titus, T.L. Foreman, M.C. Herlevsen, S.C. Smith, and D. Theodorescu,(2005) *RalA and RalB: antagonistic relatives in cancer cell migration.* Cancer Res. **65**(16): p. 7111-7120.
26. Ward, Y., W. Wang, E. Woodhouse, I. Linnoila, L. Liotta, and K. Kelly,(2001) *Signal pathways which promote invasion and metastasis: critical and distinct contributions of extracellular signal-regulated kinase and Ral-specific guanine exchange factor pathways.* Mol Cell Biol. **21**(17): p. 5958-5969.
27. Hamarsheh, S., O. Gross, T. Brummer, and R. Zeiser,(2020) *Immune modulatory effects of oncogenic KRAS in cancer.* Nat Commun. **11**(1): p. 5439.
28. Coelho, M.A., S. de Carne Trecesson, S. Rana, D. Zecchin, C. Moore, M. Molina-Arcas, P. East, B. Spencer-Dene, E. Nye, K. Barnouin, A.P. Snijders, W.S. Lai, P.J. Blackshear, and J. Downward,(2017) *Oncogenic RAS Signaling Promotes Tumor Immunoresistance by Stabilizing PD-L1 mRNA.* Immunity. **47**(6): p. 1083-1099 e1086.
29. Canon, J., K. Rex, A.Y. Saiki, C. Mohr, K. Cooke, D. Bagal, K. Gaida, T. Holt, C.G. Knutson, N. Koppada, B.A. Lanman, J. Werner, A.S. Rapaport, T. San Miguel, R. Ortiz, T. Osgood, J.R. Sun, X. Zhu, J.D. McCarter, L.P. Volak, B.E. Houk, M.G. Fakih, B.H. O'Neil, T.J. Price, G.S. Falchook, J. Desai, J. Kuo, R. Govindan, D.S. Hong, W. Ouyang, H. Henary, T. Arvedson, V.J. Cee, and J.R. Lipford,(2019) *The clinical KRAS(G12C) inhibitor AMG 510 drives anti-tumour immunity.* Nature. **575**(7781): p. 217-223.
30. McCormick, F.,(2020) *Sticking it to KRAS: Covalent Inhibitors Enter the Clinic.* Cancer Cell. **37**(1): p. 3-4.
31. Baranyi, M., L. Buday, and B. Hegedűs,(2020) *K-Ras prenylation as a potential anticancer target.* Cancer and Metastasis Reviews. **39**: p. 1127–1141.

32. Hobbs, G.A., C.J. Der, and K.L. Rossman,(2016) *RAS isoforms and mutations in cancer at a glance.* J Cell Sci. **129**(7): p. 1287-1292.
33. Potenza, N., C. Vecchione, A. Notte, A. De Rienzo, A. Rosica, L. Bauer, A. Affuso, M. De Felice, T. Russo, R. Poulet, G. Cifelli, G. De Vita, G. Lembo, and R. Di Lauro,(2005) *Replacement of K-Ras with H-Ras supports normal embryonic development despite inducing cardiovascular pathology in adult mice.* EMBO Rep. **6**(5): p. 432-437.
34. Esteban, L.M., C. Vicario-Abejon, P. Fernandez-Salguero, A. Fernandez-Medarde, N. Swaminathan, K. Yienger, E. Lopez, M. Malumbres, R. McKay, J.M. Ward, A. Pellicer, and E. Santos,(2001) *Targeted genomic disruption of H-ras and N-ras, individually or in combination, reveals the dispensability of both loci for mouse growth and development.* Mol Cell Biol. **21**(5): p. 1444-1452.
35. Umanoff, H., W. Edelmann, A. Pellicer, and R. Kucherlapati,(1995) *The murine N-ras gene is not essential for growth and development.* Proc Natl Acad Sci U S A. **92**(5): p. 1709-1713.
36. Johnson, L., D. Greenbaum, K. Cichowski, K. Mercer, E. Murphy, E. Schmitt, R.T. Bronson, H. Umanoff, W. Edelmann, R. Kucherlapati, and T. Jacks,(1997) *K-ras is an essential gene in the mouse with partial functional overlap with N-ras.* Genes Dev. **11**(19): p. 2468-2481.
37. Koera, K., K. Nakamura, K. Nakao, J. Miyoshi, K. Toyoshima, T. Hatta, H. Otani, A. Aiba, and M. Katsuki,(1997) *K-ras is essential for the development of the mouse embryo.* Oncogene. **15**(10): p. 1151-1159.
38. Yan, J., S. Roy, A. Apolloni, A. Lane, and J.F. Hancock,(1998) *Ras isoforms vary in their ability to activate Raf-1 and phosphoinositide 3-kinase.* J Biol Chem. **273**(37): p. 24052-24056.
39. Voice, J.K., R.L. Klemke, A. Le, and J.H. Jackson,(1999) *Four human ras homologs differ in their abilities to activate Raf-1, induce transformation, and stimulate cell motility.* J Biol Chem. **274**(24): p. 17164-17170.
40. Hood, F.E., B. Klinger, A.U. Newlaczyl, A. Sieber, M. Dorel, S.P. Oliver, J.M. Coulson, N. Bluthgen, and I.A. Prior,(2019) *Isoform-specific Ras signaling is growth factor dependent.* Mol Biol Cell. **30**(9): p. 1108-1117.

41. Lampson, B.L., N.L. Pershing, J.A. Prinz, J.R. Lacsina, W.F. Marzluff, C.V. Nicchitta, D.M. MacAlpine, and C.M. Counter,(2013) *Rare codons regulate KRas oncogenesis.* Curr Biol. **23**(1): p. 70-75.
42. Newlaczyl, A.U., J.M. Coulson, and I.A. Prior,(2017) *Quantification of spatiotemporal patterns of Ras isoform expression during development.* Sci Rep. **7**: p. 41297.
43. Whyte, D.B., P. Kirschmeier, T.N. Hockenberry, I. Nunez-Oliva, L. James, J.J. Catino, W.R. Bishop, and J.K. Pai,(1997) *K- and N-Ras are geranylgeranylated in cells treated with farnesyl protein transferase inhibitors.* J Biol Chem. **272**(22): p. 14459-14464.
44. Boyartchuk, V.L., M.N. Ashby, and J. Rine,(1997) *Modulation of Ras and a-factor function by carboxyl-terminal proteolysis.* Science. **275**(5307): p. 1796-1800.
45. Freije, J.M., P. Blay, A.M. Pendas, J. Cadinanos, P. Crespo, and C. Lopez-Otin,(1999) *Identification and chromosomal location of two human genes encoding enzymes potentially involved in proteolytic maturation of farnesylated proteins.* Genomics. **58**(3): p. 270-280.
46. Baranyi, M., E. Molnar, D. Rittler, B. Hegedus, and J. Timar,(2019) *[Impact of prenylation inhibition on RAS mutant tumors in preclinical studies]*. Magy Onkol. **63**(4): p. 320-329.
47. Hancock, J.F., H. Paterson, and C.J. Marshall,(1990) *A polybasic domain or palmitoylation is required in addition to the CAAX motif to localize p21ras to the plasma membrane.* Cell. **63**(1): p. 133-139.
48. Tsai, F.D., M.S. Lopes, M. Zhou, H. Court, O. Ponce, J.J. Fiordalisi, J.J. Gierut, A.D. Cox, K.M. Haigis, and M.R. Philips,(2015) *K-Ras4A splice variant is widely expressed in cancer and uses a hybrid membrane-targeting motif.* Proc Natl Acad Sci U S A. **112**(3): p. 779-784.
49. Timar, J., B. Hegedus, and E. Raso,(2010) *KRAS mutation testing of colorectal cancer for anti-EGFR therapy: dogmas versus evidence.* Curr Cancer Drug Targets. **10**(8): p. 813-823.
50. Ghimessy, A.K., A. Gellert, E. Schlegl, B. Hegedus, E. Raso, T. Barbai, J. Timar, G. Ostoros, Z. Megyesfalvi, B. Gieszer, J. Moldvay, F. Renyi-Vamos, Z.

Lohinai, M.A. Hoda, T. Klikovits, W. Klepetko, V. Laszlo, and B. Dome,(2019) *KRAS Mutations Predict Response and Outcome in Advanced Lung Adenocarcinoma Patients Receiving First-Line Bevacizumab and Platinum-Based Chemotherapy.* Cancers (Basel). **11**(10).

51. Naidoo, J. and A. Drilon,(2016) *KRAS-Mutant Lung Cancers in the Era of Targeted Therapy.* Adv Exp Med Biol. **893**: p. 155-178.
52. Singh, H., D.L. Longo, and B.A. Chabner,(2015) *Improving Prospects for Targeting RAS.* J Clin Oncol. **33**(31): p. 3650-3659.
53. Blair, H.A.,(2021) *Sotorasib: First Approval.* Drugs. **81**(13): p. 1573-1579.
54. Dunnett-Kane, V., P. Nicola, F. Blackhall, and C. Lindsay,(2021) *Mechanisms of Resistance to KRAS(G12C) Inhibitors.* Cancers (Basel). **13**(1).
55. Papke, B., S. Murarka, H.A. Vogel, P. Martin-Gago, M. Kovacevic, D.C. Truxius, E.K. Fansa, S. Ismail, G. Zimmermann, K. Heinelt, C. Schultz-Fademrecht, A. Al Saabi, M. Baumann, P. Nussbaumer, A. Wittinghofer, H. Waldmann, and P.I.H. Bastiaens,(2016) *Identification of pyrazolopyridazinones as PDEd inhibitors.* Nature Communications. **7**.
56. Noorolyai, S., N. Shajari, E. Baghbani, S. Sadreddini, and B. Baradaran,(2019) *The relation between PI3K/AKT signalling pathway and cancer.* Gene. **698**: p. 120-128.
57. Jimenez, C., C. Hernandez, B. Pimentel, and A.C. Carrera,(2002) *The p85 regulatory subunit controls sequential activation of phosphoinositide 3-kinase by Tyr kinases and Ras.* J Biol Chem. **277**(44): p. 41556-41562.
58. Rajakulendran, T., M. Sahmi, M. Lefrancois, F. Sicheri, and M. Therrien,(2009) *A dimerization-dependent mechanism drives RAF catalytic activation.* Nature. **461**(7263): p. 542-545.
59. Hibino, K., T. Shibata, T. Yanagida, and Y. Sako,(2011) *Activation kinetics of RAF protein in the ternary complex of RAF, RAS-GTP, and kinase on the plasma membrane of living cells: single-molecule imaging analysis.* J Biol Chem. **286**(42): p. 36460-36468.
60. Terrell, E.M. and D.K. Morrison,(2019) *Ras-Mediated Activation of the Raf Family Kinases.* Cold Spring Harb Perspect Med. **9**(1).

61. Ambrogio, C., J. Kohler, Z.W. Zhou, H. Wang, R. Paranal, J. Li, M. Capelletti, C. Caffarra, S. Li, Q. Lv, S. Gondi, J.C. Hunter, J. Lu, R. Chiarle, D. Santamaria, K.D. Westover, and P.A. Janne,(2018) *KRAS Dimerization Impacts MEK Inhibitor Sensitivity and Oncogenic Activity of Mutant KRAS.* Cell. **172**(4): p. 857-868 e815.

62. Spencer-Smith, R., A. Koide, Y. Zhou, R.R. Eguchi, F. Sha, P. Gajwani, D. Santana, A. Gupta, M. Jacobs, E. Herrero-Garcia, J. Cobbert, H. Lavoie, M. Smith, T. Rajakulendran, E. Dowdell, M.N. Okur, I. Dementieva, F. Sicheri, M. Therrien, J.F. Hancock, M. Ikura, S. Koide, and J.P. O'Bryan,(2017) *Inhibition of RAS function through targeting an allosteric regulatory site.* Nat Chem Biol. **13**(1): p. 62-68.

63. Nan, X., T.M. Tamguney, E.A. Collisson, L.J. Lin, C. Pitt, J. Galeas, S. Lewis, J.W. Gray, F. McCormick, and S. Chu,(2015) *Ras-GTP dimers activate the Mitogen-Activated Protein Kinase (MAPK) pathway.* Proc Natl Acad Sci U S A. **112**(26): p. 7996-8001.

64. Li, S., H. Jang, J. Zhang, and R. Nussinov,(2018) *Raf-1 Cysteine-Rich Domain Increases the Affinity of K-Ras/Raf at the Membrane, Promoting MAPK Signaling.* Structure. **26**(3): p. 513-525 e512.

65. Brock, E.J., K. Ji, J.J. Reiners, and R.R. Mattingly,(2016) *How to Target Activated Ras Proteins: Direct Inhibition vs. Induced Mislocalization.* Mini Rev Med Chem. **16**(5): p. 358-369.

66. Serna-Blasco, R., M. Sanz-Alvarez, O. Aguilera, and J. Garcia-Foncillas,(2019) *Targeting the RAS-dependent chemoresistance: The Warburg connection.* Semin Cancer Biol. **54**: p. 80-90.

67. Gilardi, M., Z. Wang, M. Proietto, A. Chilla, J.L. Calleja-Valera, Y. Goto, M. Vanoni, M.R. Janes, Z. Mikulski, A. Gualberto, A.A. Molinolo, N. Ferrara, J.S. Gutkind, and F. Burrows,(2020) *Tipifarnib as a Precision Therapy for HRAS-Mutant Head and Neck Squamous Cell Carcinomas.* Mol Cancer Ther. **19**(9): p. 1784-1796.

68. Matusewicz, L., J. Meissner, M. Toporkiewicz, and A.F. Sikorski,(2015) *The effect of statins on cancer cells--review.* Tumour Biol. **36**(7): p. 4889-4904.

69. Sivaprasad, U., T. Abbas, and A. Dutta,(2006) *Differential efficacy of 3-hydroxy-3-methylglutaryl CoA reductase inhibitors on the cell cycle of prostate cancer cells.* Mol Cancer Ther. **5**(9): p. 2310-2316.
70. Cafforio, P., F. Dammacco, A. Gernone, and F. Silvestris,(2005) *Statins activate the mitochondrial pathway of apoptosis in human lymphoblasts and myeloma cells.* Carcinogenesis. **26**(5): p. 883-891.
71. Marcelli, M., G.R. Cunningham, S.J. Haidacher, S.J. Padayatty, L. Sturgis, C. Kagan, and L. Denner,(1998) *Caspase-7 is activated during lovastatin-induced apoptosis of the prostate cancer cell line LNCaP.* Cancer Res. **58**(1): p. 76-83.
72. Song, X., B.C. Liu, X.Y. Lu, L.L. Yang, Y.J. Zhai, A.F. Eaton, T.L. Thai, D.C. Eaton, H.P. Ma, and B.Z. Shen,(2014) *Lovastatin inhibits human B lymphoma cell proliferation by reducing intracellular ROS and TRPC6 expression.* Biochim Biophys Acta. **1843**(5): p. 894-901.
73. Adhyaru, B.B. and T.A. Jacobson,(2018) *Safety and efficacy of statin therapy.* Nat Rev Cardiol. **15**(12): p. 757-769.
74. Waller, D.D., J. Park, and Y.S. Tsantrizos,(2019) *Inhibition of farnesyl pyrophosphate (FPP) and/or geranylgeranyl pyrophosphate (GGPP) biosynthesis and its implication in the treatment of cancers.* Crit Rev Biochem Mol Biol. **54**(1): p. 41-60.
75. Green, J.R.,(2004) *Bisphosphonates: preclinical review.* Oncologist. **9 Suppl 4**: p. 3-13.
76. Fragni, M., S.A. Bonini, P. Bettinsoli, S. Bodei, D. Generali, A. Bottini, P.F. Spano, M. Memo, and S. Sigala,(2016) *The miR-21/PTEN/Akt signaling pathway is involved in the anti-tumoral effects of zoledronic acid in human breast cancer cell lines.* Naunyn Schmiedebergs Arch Pharmacol. **389**(5): p. 529-538.
77. Ibrahim, T., L. Mercatali, E. Sacanna, A. Tesei, S. Carloni, P. Ulivi, C. Liverani, F. Fabbri, M. Zanoni, W. Zoli, and D. Amadori,(2012) *Inhibition of breast cancer cell proliferation in repeated and non-repeated treatment with zoledronic acid.* Cancer Cell Int. **12**(1): p. 48.
78. Mansouri, M., S.A. Mirzaei, H. Lage, S.S. Mousavi, and F. Elahian,(2014) *The cell cycle arrest and the anti-invasive effects of nitrogen-containing*

bisphosphonates are not mediated by DBF4 in breast cancer cells. Biochimie. **99**: p. 71-76.

79. Senaratne, S.G., G. Pirianov, J.L. Mansi, T.R. Arnett, and K.W. Colston,(2000) *Bisphosphonates induce apoptosis in human breast cancer cell lines.* Br J Cancer. **82**(8): p. 1459-1468.
80. Stachnik, A., T. Yuen, J. Iqbal, M. Sgobba, Y. Gupta, P. Lu, G. Colaianni, Y. Ji, L.L. Zhu, S.M. Kim, J. Li, P. Liu, S. Izadmehr, J. Sangodkar, T. Scherer, S. Mujtaba, M. Galsky, J. Gomez, S. Epstein, C. Buettner, Z. Bian, A. Zallone, A.K. Aggarwal, S. Haider, M.I. New, L. Sun, G. Narla, and M. Zaidi,(2014) *Repurposing of bisphosphonates for the prevention and therapy of nonsmall cell lung and breast cancer.* Proc Natl Acad Sci U S A. **111**(50): p. 17995-18000.
81. Di Salvatore, M., A. Orlandi, C. Bagala, M. Quirino, A. Cassano, A. Astone, and C. Barone,(2011) *Anti-tumour and anti-angiogenetic effects of zoledronic acid on human non-small-cell lung cancer cell line.* Cell Prolif. **44**(2): p. 139-146.
82. Tassone, P., P. Tagliaferri, C. Viscomi, C. Palmieri, M. Caraglia, A. D'Alessandro, E. Galea, A. Goel, A. Abbruzzese, C.R. Boland, and S. Venuta,(2003) *Zoledronic acid induces antiproliferative and apoptotic effects in human pancreatic cancer cells in vitro.* Br J Cancer. **88**(12): p. 1971-1978.
83. Tamura, T., K. Shomori, M. Nakabayashi, N. Fujii, K. Ryoke, and H. Ito,(2011) *Zoledronic acid, a third-generation bisphosphonate, inhibits cellular growth and induces apoptosis in oral carcinoma cell lines.* Oncol Rep. **25**(4): p. 1139-1143.
84. Forsea, A.M., C. Muller, C. Riebeling, C.E. Orfanos, and C.C. Geilen,(2004) *Nitrogen-containing bisphosphonates inhibit cell cycle progression in human melanoma cells.* Br J Cancer. **91**(4): p. 803-810.
85. Garay, T., I. Kenessey, E. Molnar, E. Juhasz, A. Reti, V. Laszlo, A. Rozsas, J. Dobos, B. Dome, W. Berger, W. Klepetko, J. Tovari, J. Timar, and B. Hegedus,(2015) *Prenylation inhibition-induced cell death in melanoma: reduced sensitivity in BRAF mutant/PTEN wild-type melanoma cells.* PLoS One. **10**(2): p. e0117021.

86. Yazdanifar, M., G. Barbarito, A. Bertaina, and I. Airoldi,(2020) *gammadelta T Cells: The Ideal Tool for Cancer Immunotherapy.* Cells. **9**(5).
87. Brown, H.K. and I. Holen,(2009) *Anti-tumour effects of bisphosphonates--what have we learned from in vivo models?* Curr Cancer Drug Targets. **9**(7): p. 807-823.
88. Kimmel, D.B.,(2007) *Mechanism of action, pharmacokinetic and pharmacodynamic profile, and clinical applications of nitrogen-containing bisphosphonates.* J Dent Res. **86**(11): p. 1022-1033.
89. Yuasa, T., S. Kimura, E. Ashihara, T. Habuchi, and T. Maekawa,(2007) *Zoledronic acid - a multiplicity of anti-cancer action.* Curr Med Chem. **14**(20): p. 2126-2135.
90. Miller, P.D.,(2011) *The kidney and bisphosphonates.* Bone. **49**(1): p. 77-81.
91. Xia, Y., Y.L. Liu, Y. Xie, W. Zhu, F. Guerra, S. Shen, N. Yeddula, W. Fischer, W. Low, X. Zhou, Y. Zhang, E. Oldfield, and I.M. Verma,(2014) *A combination therapy for KRAS-driven lung adenocarcinomas using lipophilic bisphosphonates and rapamycin.* Sci Transl Med. **6**(263): p. 263ra161.
92. Mitrofan, L.M., J. Pelkonen, and J. Monkkonen,(2009) *The level of ATP analog and isopentenyl pyrophosphate correlates with zoledronic acid-induced apoptosis in cancer cells in vitro.* Bone. **45**(6): p. 1153-1160.
93. Wang, M. and P.J. Casey,(2016) *Protein prenylation: unique fats make their mark on biology.* Nat Rev Mol Cell Biol. **17**(2): p. 110-122.
94. Kho, Y., S.C. Kim, C. Jiang, D. Barma, S.W. Kwon, J. Cheng, J. Jaunbergs, C. Weinbaum, F. Tamanoi, J. Falck, and Y. Zhao,(2004) *A tagging-via-substrate technology for detection and proteomics of farnesylated proteins.* Proc Natl Acad Sci U S A. **101**(34): p. 12479-12484.
95. Armstrong, S.A., V.C. Hannah, J.L. Goldstein, and M.S. Brown,(1995) *CAAX geranylgeranyl transferase transfers farnesyl as efficiently as geranylgeranyl to RhoB.* J Biol Chem. **270**(14): p. 7864-7868.
96. Rittler, D., M. Baranyi, E. Molnar, T. Garay, I. Jalsovszky, I.K. Varga, L. Hegedus, C. Aigner, J. Tovari, J. Timar, and B. Hegedus,(2019) *The Antitumor Effect of Lipophilic Bisphosphonate BPH1222 in Melanoma Models: The Role of the PI3K/Akt Pathway and the Small G Protein Rheb.* Int J Mol Sci. **20**(19).

97. Dhillon, S.,(2021) *Lonafarnib: First Approval.* Drugs. **81**(2): p. 283-289.
98. Gobel, A., M. Rauner, L.C. Hofbauer, and T.D. Rachner,(2020) *Cholesterol and beyond - The role of the mevalonate pathway in cancer biology.* Biochim Biophys Acta Rev Cancer. **1873**(2): p. 188351.
99. Mollinedo, F. and C. Gajate,(2015) *Lipid rafts as major platforms for signaling regulation in cancer.* Adv Biol Regul. **57**: p. 130-146.
100. Pike, L.J.,(2005) *Growth factor receptors, lipid rafts and caveolae: an evolving story.* Biochim Biophys Acta. **1746**(3): p. 260-273.
101. Alawin, O.A., R.A. Ahmed, B.A. Ibrahim, K.P. Briski, and P.W. Sylvester,(2016) *Antiproliferative effects of gamma-tocotrienol are associated with lipid raft disruption in HER2-positive human breast cancer cells.* J Nutr Biochem. **27**: p. 266-277.
102. Irwin, M.E., K.L. Mueller, N. Bohin, Y. Ge, and J.L. Boerner,(2011) *Lipid raft localization of EGFR alters the response of cancer cells to the EGFR tyrosine kinase inhibitor gefitinib.* J Cell Physiol. **226**(9): p. 2316-2328.
103. Azimzadeh Irani, M., S. Kannan, and C. Verma,(2017) *Role of N-glycosylation in EGFR ectodomain ligand binding.* Proteins. **85**(8): p. 1529-1549.
104. Sethi, M.K., H. Kim, C.K. Park, M.S. Baker, Y.K. Paik, N.H. Packer, W.S. Hancock, S. Fanayan, and M. Thaysen-Andersen,(2015) *In-depth N-glycome profiling of paired colorectal cancer and non-tumorigenic tissues reveals cancer-, stage- and EGFR-specific protein N-glycosylation.* Glycobiology. **25**(10): p. 1064-1078.
105. Xiao, H., G.X. Tang, and R. Wu,(2016) *Site-Specific Quantification of Surface N-Glycoproteins in Statin-Treated Liver Cells.* Anal Chem. **88**(6): p. 3324-3332.
106. Corsello, S.M., R.T. Nagari, R.D. Spangler, J. Rossen, M. Kocak, J.G. Bryan, R. Humeidi, D. Peck, X. Wu, A.A. Tang, V.M. Wang, S.A. Bender, E. Lemire, R. Narayan, P. Montgomery, U. Ben-David, C.W. Garvie, Y. Chen, M.G. Rees, N.J. Lyons, J.M. McFarland, B.T. Wong, L. Wang, N. Dumont, P.J. O'Hearn, E. Stefan, J.G. Doench, C.N. Harrington, H. Greulich, M. Meyerson, F. Vazquez, A. Subramanian, J.A. Roth, J.A. Bittker, J.S. Boehm, C.C. Mader, A. Tsherniak, and T.R. Golub,(2020) *Discovering the anticancer potential of non-oncology drugs by systematic viability profiling.* Nature Cancer. **1**(2): p. 235-248.

107. Shirasawa, S., M. Furuse, N. Yokoyama, and T. Sasazuki,(1993) *Altered growth of human colon cancer cell lines disrupted at activated Ki-ras.* Science. **260**(5104): p. 85-88.
108. Baranyi, M., D. Rittler, E. Molnar, S. Shirasawa, I. Jalsovszky, I.K. Varga, L. Hegedus, A. Nemeth, M. Dank, C. Aigner, J. Tovari, J. Timar, B. Hegedus, and T. Garay,(2020) *Next Generation Lipophilic Bisphosphonate Shows Antitumor Effect in Colorectal Cancer In Vitro and In Vivo.* Pathol Oncol Res. **26**(3): p. 1957-1969.
109. Chou, T.C.,(2010) *Drug combination studies and their synergy quantification using the Chou-Talalay method.* Cancer Res. **70**(2): p. 440-446.
110. Ivanov, D.P., T.L. Parker, D.A. Walker, C. Alexander, M.B. Ashford, P.R. Gellert, and M.C. Garnett,(2014) *Multiplexing spheroid volume, resazurin and acid phosphatase viability assays for high-throughput screening of tumour spheroids and stem cell neurospheres.* PLoS One. **9**(8): p. e103817.
111. Hegedus, L., R. Padanyi, J. Molnar, K. Paszty, K. Varga, I. Kenessey, E. Sarkozy, M. Wolf, M. Grusch, Z. Hegyi, L. Homolya, C. Aigner, T. Garay, B. Hegedus, J. Timar, E. Kallay, and A. Enyedi,(2017) *Histone Deacetylase Inhibitor Treatment Increases the Expression of the Plasma Membrane Ca2+ Pump PMCA4b and Inhibits the Migration of Melanoma Cells Independent of ERK.* Front Oncol. **7**: p. 95.
112. Janes, M.R., J.C. Zhang, L.S. Li, R. Hansen, U. Peters, X. Guo, Y.C. Chen, A. Babbar, S.J. Firdaus, L. Darjania, J. Feng, J.H. Chen, S.W. Li, S.S. Li, Y.O. Long, C. Thach, Y. Liu, A. Zarieh, T. Ely, J.M. Kucharski, L.V. Kessler, T. Wu, K. Yu, Y. Wang, Y. Yao, X.H. Deng, P.P. Zarrinkar, D. Brehmer, D. Dhanak, M.V. Lorenzi, D. Hu-Lowe, M.P. Patricelli, P.D. Ren, and Y. Liu,(2018) *Targeting KRAS Mutant Cancers with a Covalent G12C-Specific Inhibitor.* Cell. **172**(3): p. 578-+.
113. Gao, X., B. Jiang, S. Zou, T. Zhang, X. Qi, L. Jin, X. Ge, S.C. Tang, D. Hua, and W. Chen,(2015) *Zoledronate can promote apoptosis and inhibit the proliferation of colorectal cancer cells.* Tumour Biol. **36**(7): p. 5315-5322.

114. Sewing, L., F. Steinberg, H. Schmidt, and R. Göke,(2008) *The bisphosphonate zoledronic acid inhibits the growth of HCT-116 colon carcinoma cells and induces tumor cell apoptosis.* Apoptosis. **13**(6): p. 782-789.
115. Weiss, H.M., U. Pfaar, A. Schweitzer, H. Wiegand, A. Skerjanec, and H. Schran,(2008) *Biodistribution and plasma protein binding of zoledronic acid.* Drug Metab Dispos. **36**(10): p. 2043-2049.
116. Zhang, Y., R. Cao, F. Yin, M.P. Hudock, R.T. Guo, K. Krysiak, S. Mukherjee, Y.G. Gao, H. Robinson, Y. Song, J.H. No, K. Bergan, A. Leon, L. Cass, A. Goddard, T.K. Chang, F.Y. Lin, E. Van Beek, S. Papapoulos, A.H. Wang, T. Kubo, M. Ochi, D. Mukkamala, and E. Oldfield,(2009) *Lipophilic bisphosphonates as dual farnesyl/geranylgeranyl diphosphate synthase inhibitors: an X-ray and NMR investigation.* J Am Chem Soc. **131**(14): p. 5153-5162.
117. Kato, J., M. Futamura, M. Kanematsu, S. Gaowa, R. Mori, T. Tanahashi, N. Matsuhashi, and K. Yoshida,(2016) *Combination therapy with zoledronic acid and cetuximab effectively suppresses growth of colorectal cancer cells regardless of KRAS status.* Int J Cancer. **138**(6): p. 1516-1527.
118. Nath, S. and G.R. Devi,(2016) *Three-dimensional culture systems in cancer research: Focus on tumor spheroid model.* Pharmacology & Therapeutics. **163**: p. 94-108.
119. Kelsey, I. and B.D. Manning,(2013) *mTORC1 status dictates tumor response to targeted therapeutics.* Sci Signal. **6**(294): p. pe31.
120. Kopetz, S., J. Desai, E. Chan, J.R. Hecht, P.J. O'Dwyer, D. Maru, V. Morris, F. Janku, A. Dasari, W. Chung, J.P. Issa, P. Gibbs, B. James, G. Powis, K.B. Nolop, S. Bhattacharya, and L. Saltz,(2015) *Phase II Pilot Study of Vemurafenib in Patients With Metastatic BRAF-Mutated Colorectal Cancer.* J Clin Oncol. **33**(34): p. 4032-4038.
121. Schneider, G., M. Schmidt-Supprian, R. Rad, and D. Saur,(2017) *Tissue-specific tumorigenesis: context matters.* Nat Rev Cancer. **17**(4): p. 239-253.
122. Lohinai, Z., T. Klikovits, J. Moldvay, G. Ostoros, E. Raso, J. Timar, K. Fabian, I. Kovalszky, I. Kenessey, C. Aigner, F. Renyi-Vamos, W. Klepetko, B. Dome, and B. Hegedus,(2017) *KRAS-mutation incidence and prognostic value are*

metastatic site-specific in lung adenocarcinoma: poor prognosis in patients with KRAS mutation and bone metastasis. Sci Rep. **7**: p. 39721.

123. Kanaji, N., A. Tadokoro, N. Watanabe, T. Inoue, N. Kadowaki, and T. Ishii,(2019) *Association of specific metastatic organs with the prognosis and chemotherapeutic response in patients with advanced lung cancer.* Respir Investig. **57**(5): p. 472-480.

124. Kuijpers, C., L.E.L. Hendriks, J.L. Derks, A.C. Dingemans, A.S.R. van Lindert, M.M. van den Heuvel, R.A. Damhuis, and S.M. Willems,(2018) *Association of molecular status and metastatic organs at diagnosis in patients with stage IV non-squamous non-small cell lung cancer.* Lung Cancer. **121**: p. 76-81.

125. Timar, J.,(2014) *The clinical relevance of KRAS gene mutation in non-small-cell lung cancer.* Curr Opin Oncol. **26**(2): p. 138-144.

126. Moghadamchargari, Z., J. Huddleston, M. Shirzadeh, X. Zheng, D.E. Clemmer, M.R. F, D.H. Russell, and A. Laganowsky,(2019) *Intrinsic GTPase Activity of K-RAS Monitored by Native Mass Spectrometry.* Biochemistry. **58**(31): p. 3396-3405.

127. Zhang, F.L., P. Kirschmeier, D. Carr, L. James, R.W. Bond, L. Wang, R. Patton, W.T. Windsor, R. Syto, R. Zhang, and W.R. Bishop,(1997) *Characterization of Ha-ras, N-ras, Ki-Ras4A, and Ki-Ras4B as in vitro substrates for farnesyl protein transferase and geranylgeranyl protein transferase type I.* J Biol Chem. **272**(15): p. 10232-10239.

128. Tew, G.W., E.L. Lorimer, T.J. Berg, H. Zhi, R. Li, and C.L. Williams,(2008) *SmgGDS regulates cell proliferation, migration, and NF-kappaB transcriptional activity in non-small cell lung carcinoma.* J Biol Chem. **283**(2): p. 963-976.

129. Schuld, N.J., A.D. Hauser, A.J. Gastonguay, J.M. Wilson, E.L. Lorimer, and C.L. Williams,(2014) *SmgGDS-558 regulates the cell cycle in pancreatic, non-small cell lung, and breast cancers.* Cell Cycle. **13**(6): p. 941-952.

130. Brandt, A.C., L. McNally, E.L. Lorimer, B. Unger, O.J. Koehn, K.F. Suazo, L. Rein, A. Szabo, S.W. Tsaih, M.D. Distefano, M.J. Flister, F. Rigo, M.T. McNally, and C.L. Williams,(2020) *Splice switching an oncogenic ratio of SmgGDS isoforms as a strategy to diminish malignancy.* Proc Natl Acad Sci U S A. **117**(7): p. 3627-3636.

131. Shukla, S., U.S. Allam, A. Ahsan, G. Chen, P.M. Krishnamurthy, K. Marsh, M. Rumschlag, S. Shankar, C. Whitehead, M. Schipper, V. Basrur, D.R. Southworth, A.M. Chinnaiyan, A. Rehemtulla, D.G. Beer, T.S. Lawrence, M.K. Nyati, and D. Ray,(2014) *KRAS protein stability is regulated through SMURF2: UBCH5 complex-mediated beta-TrCP1 degradation.* Neoplasia. **16**(2): p. 115-128.

132. Zeng, T., Q. Wang, J. Fu, Q. Lin, J. Bi, W. Ding, Y. Qiao, S. Zhang, W. Zhao, H. Lin, M. Wang, B. Lu, X. Deng, D. Zhou, Z. Yin, and H.R. Wang,(2014) *Impeded Nedd4-1-mediated Ras degradation underlies Ras-driven tumorigenesis.* Cell Rep. **7**(3): p. 871-882.

133. Steklov, M., S. Pandolfi, M.F. Baietti, A. Batiuk, P. Carai, P. Najm, M. Zhang, H. Jang, F. Renzi, Y. Cai, L. Abbasi Asbagh, T. Pastor, M. De Troyer, M. Simicek, E. Radaelli, H. Brems, E. Legius, J. Tavernier, K. Gevaert, F. Impens, L. Messiaen, R. Nussinov, S. Heymans, S. Eyckerman, and A.A. Sablina,(2018) *Mutations in LZTR1 drive human disease by dysregulating RAS ubiquitination.* Science. **362**(6419): p. 1177-1182.

134. Lee, S.K., W.J. Jeong, Y.H. Cho, P.H. Cha, J.S. Yoon, E.J. Ro, S. Choi, J.M. Oh, Y. Heo, H. Kim, D.S. Min, G. Han, W. Lee, and K.Y. Choi,(2018) *beta-Catenin-RAS interaction serves as a molecular switch for RAS degradation via GSK3beta.* EMBO Rep. **19**(12).

135. Jeong, W.J., E.J. Ro, and K.Y. Choi,(2018) *Interaction between Wnt/beta-catenin and RAS-ERK pathways and an anti-cancer strategy via degradations of beta-catenin and RAS by targeting the Wnt/beta-catenin pathway.* NPJ Precis Oncol. **2**(1): p. 5.

136. Timar, J., B. Hegedus, and E. Raso,(2010) *KRAS Mutation Testing of Colorectal Cancer for Anti-EGFR Therapy: Dogmas Versus Evidence.* Current Cancer Drug Targets. **10**(8): p. 813-823.

137. Hong, D.S., M.G. Fakih, J.H. Strickler, J. Desai, G.A. Durm, G.I. Shapiro, G.S. Falchook, T.J. Price, A. Sacher, C.S. Denlinger, Y.J. Bang, G.K. Dy, J.C. Krauss, Y. Kuboki, J.C. Kuo, A.L. Coveler, K. Park, T.W. Kim, F. Barlesi, P.N. Munster, S.S. Ramalingam, T.F. Burns, F. Meric-Bernstam, H. Henary, J. Ngang, G. Ngarmchamnanrith, J. Kim, B.E. Houk, J. Canon, J.R. Lipford, G.

Friberg, P. Lito, R. Govindan, and B.T. Li,(2020) *KRAS(G12C) Inhibition with Sotorasib in Advanced Solid Tumors.* N Engl J Med. **383**(13): p. 1207-1217.

138. Appels, N.M., J.H. Beijnen, and J.H. Schellens,(2005) *Development of farnesyl transferase inhibitors: a review.* Oncologist. **10**(8): p. 565-578.
139. Hallin, J., L.D. Engstrom, L. Hargis, A. Calinisan, R. Aranda, D.M. Briere, N. Sudhakar, V. Bowcut, B.R. Baer, J.A. Ballard, M.R. Burkard, J.B. Fell, J.P. Fischer, G.P. Vigers, Y. Xue, S. Gatto, J. Fernandez-Banet, A. Pavlicek, K. Velastagui, R.C. Chao, J. Barton, M. Pierobon, E. Baldelli, E.F. Patricoin, 3rd, D.P. Cassidy, M.A. Marx, Rybkin, II, M.L. Johnson, S.I. Ou, P. Lito, K.P. Papadopoulos, P.A. Janne, P. Olson, and J.G. Christensen,(2020) *The KRAS(G12C) Inhibitor MRTX849 Provides Insight toward Therapeutic Susceptibility of KRAS-Mutant Cancers in Mouse Models and Patients.* Cancer Discov. **10**(1): p. 54-71.
140. Berndt, N. and S.M. Sebti,(2011) *Measurement of protein farnesylation and geranylgeranylation in vitro, in cultured cells and in biopsies, and the effects of prenyl transferase inhibitors.* Nat Protoc. **6**(11): p. 1775-1791.
141. Shinde, S.R. and S. Maddika,(2018) *Post translational modifications of Rab GTPases.* Small GTPases. **9**(1-2): p. 49-56.

10. Bibliography of the candidate's publications

List of publications related to the thesis

M. Baranyi, L. Buday, and B. Hegedűs, KRas prenylation as a potential anticancer target. Cancer and Metastasis Reviews, 2020. 39: p. 1127–1141.**IF:9,264, Q1**

M. Baranyi, D. Rittler, E. Molnár, S. Shirasawa, I. Jalsovszky, I. K. Varga, L. Hegedűs, A. Németh, M. Dank, C. Aigner, J. Tóvári, J. Tímár, B. Hegedűs, T. Garay, Next Generation Lipophilic Bisphosphonate Shows Antitumor Effect in Colorectal Cancer In Vitro and In Vivo. Pathol Oncol Res, 2020. 26(3): p. 1957-1969. **IF: 3,201, Q2**

Patent: Combination therapy to treat G12C KRAS mutant cancers; **PATENT REGISTRATION NUMBER: 133077, CASE NUMBER: P 21 00375**; Inventors: J. Tímár; B. Hegedűs; M.Baranyi; E. Molnár; J. Tóvári; I. Randelovic

M. Baranyi; E.Molnar; D. Rittler;; B.Hegedus; J. Timar; Prenilációgátlás hatása RAS-mutáns daganatokra kísérleti rendszerekben [Impact of prenylation inhibition on RAS mutant tumors in preclinical studies]; MAGYAR ONKOLÓGIA 63 : 4 pp. 320-329. , 10 p. (2019) **IF:0**

Other publications that are not part of this thesis

Hegedüs, L. ; Okumus, Ö. ; Livingstone, E. ; **Baranyi, M**. ; Kovács, I. ; Döme, B. ; Tóvári, J. ; Bánkfalvi, Á. ; Schadendorf, D. ; Aigner, C. et al; Allosteric and ATP-competitive MEK-inhibition in a novel spitzoid melanoma model with a raf-and phosphorylation-independent mutation; *Cancers* 13 : 4 Paper: 829 , 12 p. (2021**) IF: 6.639**

D. Rittler; E.Molnar,; **M. Baranyi**,; T.Garay; L. Hegedus; C. Aigner,; J. Tovari,; J. Timar,; B.Hegedus; Horizontal Combination of MEK and PI3K/mTOR Inhibition in BRAF Mutant Tumor Cells with or without Concomitant PI3K Pathway Mutations;

International Journal of Molecular Sciences 21 : 20 Paper: 7649 , 18 p. (2020) **IF: 5.924**

E.Molnar; T.Garay; M. Donia; **M. Baranyi**; D. Rittler; W. Berger; J. Timar; M. Grusch; B.Hegedus;; Long-Term Vemurafenib Exposure Induced Alterations of Cell Phenotypes in Melanoma: Increased Cell Migration and Its Association with EGFR Expression; *International Journal of Molecular Sciences* 20 : 18 Paper: 4484 , 13 p. (2019) **IF: 4.556**

K. Nyíri; G.Koppány; Gy. Pálfy; I. Vida; Sz. Tóth; Z. Orgován; I. Ranđelović; **M. Baranyi**; E.Molnar; Gy. M. Keserű, et al. Allélspecifikus inhibitorok nyomában: a RASopátia konzorcium célpontjában a KRAS fehérje onkogén mutációi [Allele-specific inhibitors of mutant kras are in the focus of rasopathy consortium]; *Magyar Onkológia* 63 : 4 pp. 310-323., 10 p. (2019) **IF: 0**

D. Rittler; E.Molnar,; **M. Baranyi**; E.Molnar; T.Garay; I. Jalsovszky, I. K. Varga ; L. Hegedus; C. Aigner,; J. Tovari,; J. Timar,et al.The Antitumor Effect of Lipophilic Bisphosphonate BPH1222 in Melanoma Models: The Role of the PI3K/AKT Pathway and the Small G Protein RHEB; *International Journal of Molecular Sciences* 20 : 19 p. 4917 , 15 p. (2019) **IF: 4.556**

E.Molnar; D. Rittler; **M. Baranyi**; M. Grusch; W.Berger,; B.Dome; J.Tovari, ; C. Aigner; J.Timar; T.Garay, ** et al.; Pan-RAF and MEK vertical inhibition enhances therapeutic response in non-V600 BRAF mutant cells; BMC CANCER 18 : 1 Paper: 542 , 11 p. (2018) **IF: 2,933**

A.Gaál,; V.G. Mihucz; Sz. Bősze; I. Szabó; **M. Baranyi**; P. Horváth; C. Streli; N. Szoboszlai; Comparative in vitro investigation of anticancer copper chelating agents; *Microchemical Journal* 136 pp. 227-235. , 9 p. (2018) **IF: 3,206**

M. Baranyi; M. Lippai ; Zs. Szatmari; A stroma szerepe a tumorok kialakulásában és progressziójaban.; *Orvosi Hetilap* 156 : 45 pp. 1816-1823. , 8 p. (2015) **IF: 0.291**

11. Köszönetnyilvánítás

Szeretném kifejezni a köszönetemet mindazoknak, akik segítsége és támogatása nélkül nem jöhetett volna létre ez a doktori munka. Elsősorban Tímár József professzor úrnak szeretném megköszönni az elmúlt években nyújtott minden támogatását, segítségét és a témavezetői munkáját, amellyel lehetővé tette és ösztönözte a kutatásaimat. Hálával tartozom Dr. Hegedűs Balázsnak, akinek tanácsai és példája nagyon sokat jelentettek számomra.

Köszönöm Dominak és Eszternek a rengeteg támogatást és a laboratóriumban kialakult bátorító és megtartó légkört, nagyon szerencsésnek érzem magam, hogy éveken keresztül ilyen környezetben dolgozhattam. Köszönöm a „tágabb labornak" Bilecz Áginak, Anikónak, Tamásnak, Tózsinak, Anitának, Vittinek és Ivánnak az elmúlt évek minden segítségét és támogatását. Köszönöm a kollaborátorainknak, barátainknak minden segítségét: a Ca2+ munkacsoport jelenlegi és volt tagjaitól, az Onkológiai Intézet és az I.Pathológiai Intézet munkatársaitól kapott minden segítséget. Kiemelten köszönöm a II. Pathológiai Intézet munkatársaitól kapott minden támogatást és segítséget a teljesség igénye nélkül; Dr. Lotz Gábortól, Piurkó Violettától, Dr. Kocsmár Évitől és Ilditől, Dr. Lendvai Gábortól és Dr. Tőkés Anna-Máriától.

Köszönöm feleségem, szüleim, testvéreim, barátaim minden szeretetét, bátorítását és elismerését, amely nélkül nem lennék az, aki vagyok. Leginkább pedig köszönöm Isten szeretetét és gondoskodását, hogy ennyi rendkívüli emberrel vett engem körül.